

# FAST MOLECULAR REORIENTATION IN LIQUID CRYSTALS PROBED BY NONLINEAR OPTICS

J. R. LALANNE

*CNRS Paul Pascal, Pessac, France*

J. BUCHERT

*IUSL City of College of New York, New York, New York*

S. KIELICH

*Nonlinear Optics Department, Adam Mickiewicz University,  
Poznań, Poland*

## CONTENTS

- I. Introduction
- II. General Considerations
  - A. Third-Order Interaction Between a Laser Field  $E(\mathbf{r}, t)$  and Matter (Assumed to Be Macroscopically Isotropic)
  - B. Comparison Between the Electronic and Orientational Contributions
  - C. Definition of the First-Order Polarizability Anisotropy  $\gamma$
  - D. The Link Between Nonlinear Optical Properties Described by  $\chi_{(1)\text{ani}}^{(3)}$  and Those Probed by Depolarized Rayleigh Scattering (DRS)
  - E. Relation Between Various Relaxation Times
- III. Nonlinear Optical Techniques Used for the Study of Fast Molecular Relaxations in Liquid Crystals
  - A. Optical Kerr Effect
  - B. Induced Transient Grating
  - C. Degenerate Four-Wave Mixing
- IV. The Liquid Crystals and Their Preparation
  - A. Structure of the Phases
  - B. The Compounds Studied

---

*Modern Nonlinear Optics, Part 1*, Edited by Myron Evans and Stanisław Kielich. Advances in Chemical Physics Series, Vol. LXXXV.  
ISBN 0-471-57546-1 © 1993 John Wiley & Sons, Inc.

vectors of the components.  $P_i^3(\mathbf{r}, t)$  can be written [29] as

$$\begin{aligned}
 P_i^3(\omega_\Sigma) = & \sum_{a,b,c} E_j^{\omega_a} \exp[i(\mathbf{k}_a + \mathbf{k}_b + \mathbf{k}_c) \cdot \mathbf{r} - \omega_\Sigma t] \\
 & \times \left[ \chi_{\text{iso}}^{(3)}(-\omega_\Sigma, \omega_a, \omega_b, \omega_c) \delta_{ij} E_k^{\omega_b} E_k^{\omega_c} \right. \\
 & + \chi_{\text{ani}}^{(3)}(-\omega_\Sigma, \omega_a, \omega_b, \omega_c) \left( \frac{3}{2} E_i^{\omega_b} E_j^{\omega_c} \right. \\
 & \left. \left. + \frac{3}{2} E_j^{\omega_b} E_i^{\omega_c} - \delta_{ij} E_k^{\omega_b} E_k^{\omega_c} \right) \right] \quad (3)
 \end{aligned}$$

where  $\omega_a = 2\pi c/\lambda_a$ ,  $\omega_b = 2\pi c/\lambda_b$ ,  $\omega_c = 2\pi c/\lambda_c$  are the frequencies of the fields corresponding to the related wavelengths  $\lambda$ ;  $c$  is the speed of light; and  $\omega_\Sigma$  denotes the frequencies sum ( $\omega_a + \omega_b + \omega_c$ ).  $\chi_{\text{iso}}^{(3)}$  and  $\chi_{\text{ani}}^{(3)}$  respectively describe the isotropic and anisotropic parts of the optical nonlinearities. In fact, they are statistical parameters, functions of the temperature which can be written, by use of perturbation theory, in the form

$$\chi^{(3)}(T) = \sum_n \chi_{(n)}^{(3)} T^{(-n)} \quad (4)$$

The first two orders  $n = 0$  and  $n = 1$  are of great interest within the framework of this work:

1. *Zero-order approximation.* In this case  $\chi_{(0)}^{(3)}$  is temperature independent and describes pure electronic phenomena, classically described about 100 years ago by Voigt [30], and later by Born [31] and Buckingham [24]. If one assumes that the molecular third-order tensor  $C_{\alpha\beta\gamma\delta}$  is symmetric in the indexes  $\alpha, \beta, \gamma, \delta$ , one finds

$$\chi_{(0)\text{iso}}^{(3)} = \frac{5}{2} \chi_{(0)\text{ani}}^{(3)} = \frac{1}{18} \rho C_{\alpha\alpha\beta\beta} \quad (5)$$

where  $\rho$  is the number density of molecules. This will be the case for all the liquid crystal molecules studied, because our choice of laser optical frequencies is very far from the electronic absorption ones. This effect can be viewed as an induced deformation of the electron clouds by the field. The associated times are expected to be in the  $10^{-15}$ -s range.

2. *First-order approximations.* A complete treatment can be deduced from Debye's famous work [32]. In our case, limited to orientational phenomena induced by laser fields, we can neglect the interaction of permanent electric dipoles with the optical field. A very simple explanation was proposed by Mayer and Gires [25] in the 1960s: The

time-averaged orientational torque vanishes because of the incapability of the permanent dipoles to “follow” the optical field. In this case, we find

$$\chi_{(1)\text{iso}}^{(3)}(-\omega_{\Sigma}, \omega_a, \omega_b, \omega_c) = 0 \quad (6)$$

$$\chi_{(1)\text{ani}}^{(3)}(-\omega_{\Sigma}, \omega_a, \omega_b, \omega_c) = \frac{2\rho}{45k} \frac{\gamma(-\omega_{\Sigma}, \omega_a)\gamma(\omega_b, \omega_c)}{1 - i(\omega_b + \omega_c)\tau_2} \quad (7)$$

where  $k$  is the Boltzmann constant and  $\gamma$  is the anisotropy of the first-order polarizability  $\alpha$ , which will be defined further on.  $\tau_2$  is connected with the Debye time  $\tau_D$  by  $\tau_2 = \tau_D/3$ . For ordinary molecules,  $\tau_D$  is about  $10^{-11}$  s, leading to values of  $\tau_2$  in the picosecond range. Extended theory [33], which is not reported here, shows that time  $\tau_2$  also characterizes rise and decay processes in the medium. The second and third approximations contribute nothing in our case, and we immediately understand why picosecond laser pulses are mainly qualified to probe, by analysis in real time, pseudo-individual molecular reorientations, which exhibit  $\tau_2$  values in the same range of time of the pulse duration. However, the responses of liquid crystals to picosecond optical pulses integrate the electronic contributions and it is important to know their magnitude.

### B. Comparison Between the Electronic and Orientational Contributions

For usual molecules, such as  $\text{CS}_2$ , electronic deformation is about  $10^{-36}$  esu [34], while  $\gamma^2$  is about  $10^{-46}$   $\text{cm}^6$  [35], leading to a value of the ratio  $\chi_{(0)\text{iso}}^{(3)}/\chi_{(0)\text{ani}}^{(3)}$  about  $5 \times 10^{-4}$  at room temperature. Such values can be obtained for a large number of organic molecules, with a framework not very different from that of liquid crystals molecules [34].

We have measured [36]  $\gamma^2$  in 4-cyano-4-*n*-octylbiphenyl (8CB) in cyclohexane diluted solution [36] and found  $\gamma^2 \approx 9 \times 10^{-46}$   $\text{cm}^6$  from an experiment of depolarized Rayleigh scattering performed at a wavelength of 510 nm, i.e., at approximately the same frequency as those used in nonlinear optics (532 nm). This value is about nine times larger than the corresponding one for  $\text{CS}_2$ .

Recent measurements [37] of the nonlinear part of the refractive index in 5CB (4-cyano-4'-*n*-pentylcyanobiphenyl), performed by the so-called Z-scan technique [38], using 33-ps pulses, gives values of the nonlinear parts of the refractive index (at 532 nm)  $n_{2\parallel} = 1.04 \times 10^{-11}$  esu and  $n_{2\perp} = 0.69 \times 10^{-11}$  esu (the subscripts  $\parallel$  and  $\perp$  respectively refer to light polarized parallel and perpendicular to the director of the oriented sample

at 24°C, i.e., in the nematic phase). The values are smaller than that of CS<sub>2</sub>, which is about  $1.1 \times 10^{-11}$  esu [34], thus confirming results obtained some years ago [39, 40].

Because the nonlinear part  $n_2$  is directly proportional to the electronic third polarizability  $C$ , it can be easily calculated that  $C$  is about  $10^{-36}$  esu for 5CB in the nematic state. This experimental value is about three orders of magnitude smaller than the result of a recent calculation on the cyanobiphenyl series, using Parr, Pariser and Pople or Huckel approximations [41], which predicts the electronic contribution of the mean third-order polarizability to be about  $10^{-33}$  esu. Such high polarizabilities are, in fact, measured only for large molecules having high conjugation [42] in their central framework and appear to be unrealistic in the case of liquid crystals. Recent measurements performed in a series of naphthyl-core liquid crystals also lead to values of  $\chi^{(3)}$  largely inferior to the ones of CS<sub>2</sub>. Electronic contributions are neglected in studies using pulses of some tens of picoseconds.

### C. Definition of the First-Order Polarizability Anisotropy $\gamma$

$\gamma^2$  is defined by  $\gamma^2 = \frac{3}{2}[\text{Tr}(\alpha\alpha) - \frac{1}{3}(\text{Tr}\alpha)^2]$ , where  $\alpha$  is the first-order polarizability and Tr defines the trace of the second-order tensor  $\alpha$ . When applied in the principal frame of the molecule, this last relation leads to [43]

$$\gamma^2 = \frac{1}{2}[(\alpha_{\parallel} - \alpha_{\perp,1})^2 + (\alpha_{\parallel} - \alpha_{\perp,2})^2 + (\alpha_{\perp,1} - \alpha_{\perp,2})^2] \quad (8)$$

where  $\alpha_{\parallel}$  is the principal polarizability along the long axis of the molecule, and  $\alpha_{\perp,1}$  and  $\alpha_{\perp,2}$  the ones in the planes perpendicular to this axis. It is often admitted that  $\alpha_{\parallel} \gg \alpha_{\perp,1} = \alpha_{\perp,2}$  then the molecule is assumed to be optically rodlike. Such an assumption is always highly unrealistic: By assuming that the C<sub>8</sub>H<sub>17</sub> chain of 8 CB has an isotropic first-order polarizability in the plane perpendicular to the long molecular axis, we have been able to calculate [36]  $\gamma_{\perp}^2 = (\alpha_{\perp,1} - \alpha_{\perp,2})^2$  for 8 CB and found the very large value  $441 \times 10^{-48}$  cm<sup>6</sup> (which is still four times larger than that of  $\gamma^2 = (\alpha_{\parallel} - \alpha_{\perp})^2$  in CS<sub>2</sub>). This point appears to be important, because it explains why an optical polarized field can produce molecular orientational effects in oriented liquid crystal samples where the director of the phase is parallel to the wave vector of the light (see Section V). All the effects described in this paper should not exist in oriented *N* and *Sm-A* phases composed of rod like molecules.

The parameter  $\gamma^2$ , which has been intensively studied for nematogens—where it determines the birefringence of the nematic directly connected

to display performance—cannot be considered here as an intrinsic molecular parameter. Strongly connected with the *local* orientational order [44] in the fluid and with the shape of the cavity used for the evaluation of the so-called local field  $\mathcal{L}$  [45], it should be considered as an effective parameter and should be written  $\mathcal{L} \gamma_{\text{eff}}^2$ . Molecular theories [46, 47] of  $\mathcal{L}$  suggest an expression of the form  $\mathcal{L} = [(n^2 + 2)/3]^4$ , where  $n$  is the refractive index. The expression of  $\gamma_{\text{eff}}^2$  is difficult to write in the general case of asymmetric molecules. Flygare et al. [48] proposed an expression that can be written

$$\gamma_{\text{eff}}^2 = N_{11} \Delta\alpha_1^2 + 2N_{22} \Delta\alpha_2^2 + 2\sqrt{2}N_{12} \Delta\alpha_1 \Delta\alpha_2 \quad (9)$$

where  $\Delta\alpha_1$  and  $\Delta\alpha_2$  are polarizability anisotropies that can be expressed in terms of the components of the so-called principal first-order polarization tensor of the molecule:

$$\begin{aligned} \Delta\alpha_1 &= \frac{1}{2}(2\alpha_{\perp} - \alpha_{\parallel,1} - \alpha_{\perp,2}) \\ \Delta\alpha_2 &= \frac{1}{2}(\alpha_{\perp,1} - \alpha_{\perp,2}) \end{aligned} \quad (10)$$

The first term of Eq. (9) is the most important and can be written

$$N_{11} \Delta\alpha_1^2 = \gamma^2 [1 + (N - 1) \langle D_{00}^{(2)}(1) D_{00}^{(2)}(2) \rangle] \quad (11)$$

where  $N$  is the number of molecules in the scattering volume and  $D_{00}^{(2)}(i)$  are the second-order Wigner rotation functions [49] of the Euler angles that describe the orientation of molecule  $i$  expressed in the laboratory coordinate system. The brackets indicate the space average. The  $D_{km}^{(l)}(\Omega)$  Wigner functions are introduced in the generalized Van Hove correlation function [50]  $G(\mathbf{r}, \Omega, t)$ , which can be expanded in terms of a complete set of Wigner functions ( $\Omega$  here is the orientational parameter). In the case of rodlike molecules  $\Delta\alpha_1 = \alpha_{\parallel} - \alpha_{\perp} = \gamma$ ;  $\Delta\alpha_2 = 0$  and Eq. 12 leads to the well-known expression [51]

$$\gamma_{\text{eff}}^2 = \gamma^2(1 + J_A) \quad (12)$$

with

$$J_A = (N - 1) \langle \frac{3}{2} \cos^2 \theta_{ij} - \frac{1}{2} \rangle \quad (13)$$

where  $\theta_{ij}$  is the angle between the different  $C_{\infty}$  axes of the molecules.

TABLE I  
Relative Values of  $\chi_{(1)}^{(3)}$  and  $\gamma_{\text{eff}}^2$  Versus Temperature for Simple Molecules  
Used in the Central Framework of Liquid Crystals

Compound	$T$ (K) ( $\pm 0.1$ )	$d$ (g/cm <sup>3</sup> ) ( $\pm 0.001$ )	$n$ (632.8 nm) ( $\pm 10^{-4}$ )	$n$ (1060 nm) ( $\pm 10^{-4}$ )	$\frac{\chi_{(1)}^{(3)}(T)}{\chi_{(1)}^{(3)}(T_0)}$	$\frac{\gamma_{\text{eff}}^2(T)}{\gamma_{\text{eff}}^2(T_0)}$
Benzene	294	0.872	1.4969	1.4902	1	1
	328.5	0.841	1.4775	1.4708	0.94	1.12
	342	0.827	1.4699	1.4629	0.97	1.24
Toluene	294	0.867	1.4933	1.4812	1	1
	324	0.838	1.4775	1.4662	0.87	1.01
	353	0.817	1.4628	1.4519	0.78	1.04
Nitrobenzene	294	1.203	1.5473	1.5277	1	1
	314.2	1.182	1.5384	1.5203	0.90	0.99
	328.5	1.166	1.5321	1.5151	0.84	0.98
	343	1.151	1.5257	1.5098	0.75	0.94
	357	1.136	1.5197	1.5047	0.69	0.92

Note. The nonlinear technique used is OKE. The reference temperature is 294 K. The wavelengths used are  $\lambda_a = 632.8$  nm,  $\lambda_b = \lambda_c = 1060$  nm (see Eq. 4).  $d$  is the density.

In the general case, the parameters  $N_{22}$  and  $N_{21}$  are difficult to calculate. The variations of the orientational local order with temperature are also barely predictable. However, previous work [51] performed on simple molecules shows that the local angular correlations between anisotropic molecules can be rather important. In the case of nitrobenzene, we have found  $\gamma_{\text{eff}}^2/\gamma^2 = 2.2 \pm 0.1$  (this value can be compared to the corresponding one ( $2.8 \pm 0.3$ ) obtained by Alms et al. [44]). These correlations are in general temperature dependent. We illustrate this point by reporting results obtained on three anisotropic molecules basically used in the central framework in liquid crystals [52]. The measured values of useful physical parameters are listed in Table I.

These results are reported in Fig. 1 and are different for the three liquids studied. For toluene the decrease of  $\chi_{(1)}^{(3)}$  with temperature (22%, from 293 to 353 K) is exactly as predicted by the  $1/T$  temperature dependence (Fig. 1a).  $\gamma_{\text{eff}}^2$  appears to be temperature independent (atropic behavior) (Fig. 1b). For benzene and nitrobenzene the  $1/T$  law is not fulfilled (Fig. 1a) leading to  $\gamma_{\text{eff}}^2$  respectively increasing and decreasing functions of the temperature (Fig. 1b). These two behaviors are respectively denoted diatropism and paratropism [51], and can be important. For nitrobenzene, the OKE signal, which varies as the squared value of  $\chi_{(1)}^{(3)}$ , is divided by a factor about two from 294 to 357 K. In this case, the short-range molecular organization (paratropic tendency to a parallel

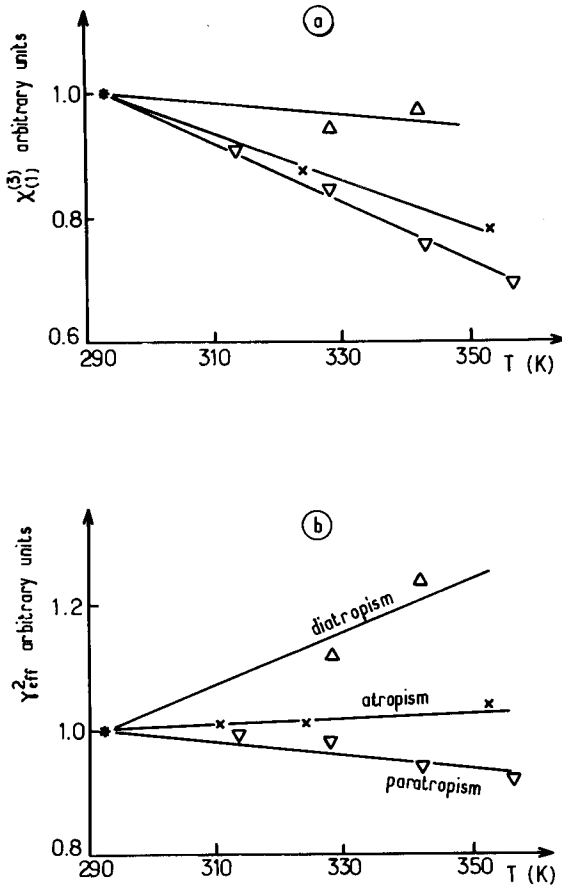


**Figure 1.** Variations of (a)  $\chi_{(1)}^{(3)}$  and (b)  $\gamma_{\text{eff}}^2$  versus temperature. The values are referred to the corresponding one at  $T = 294$  K;  $\Delta$ , benzene;  $\nabla$ , nitrobenzene;  $\times$ , toluene.

organization) is progressively destroyed when the temperature rises and the effective optical anisotropy decreases. The comparison of these preliminary results to corresponding results obtained in liquid crystals should thus be fruitful.

#### D. The Link Between Nonlinear Optical Properties Described by $\chi_{(1)\text{ani}}^{(3)}$ and Those Probed by Depolarized Rayleigh Scattering (DRS)

The intensity of the depolarized scattered light from liquids composed of optically anisotropic molecules can be used to measure polarizability

anisotropies and angular pair correlations between particles in dense fluids and solutions [35]. Starting with vertically ( $V$ ) polarized incident light (frequency  $\omega_R$ ), the intensity of the depolarized light  $I_{VH}$  (electric field in a horizontal ( $H$ ) plane) scattered by spatially isotropic fluids appears to be basically proportional to  $\gamma^2(-\omega_R, \omega_R)$ . This parameter includes a summation (over the molecules in the scattering volume) of the second-order spherical harmonic, which describes the orientation of the molecules and is then directly connected to the short-range orientational order of the medium. Then, if as previously assumed, the electronic contribution can be neglected in the induced third-order polarization, nonlinear optical techniques measuring  $\chi_{(1)\text{ani}}^{(3)}$  (Eq. (8)) and depolarized Rayleigh scattering lead to the same parameter  $\gamma^2$ , directly connected to the local molecular orientational order of the fluid. The proof of such a conclusion can be found from experimental work concerning strongly anisotropic simple liquids [53].

Table II reports our contribution in this domain. All the measurements relate to benzene. Comparison between the two columns on the right in Table II shows that, taking into account the experimental errors, there is rather good agreement between the two kinds of results, when they are corrected for the dispersion [54] due to the experimental use of different frequencies. This agreement is important because it allows us to directly compare results obtained in liquid crystals by NLO techniques and by Rayleigh scattering. The latter has often been used recently in liquid crystal research.

Moreover, Rayleigh light-scattering techniques can be used not only to determine the degree of orientational order in liquids and to provide

TABLE II  
Comparison Between Nonlinear Optical Techniques and DRS results

Liquid	$\chi_{(1)\text{ani}}^{(3)}/\chi_{(1)\text{ani, benz}}^{(3)}$			$\frac{\chi_{(1)\text{ani}}^{(3)}}{\chi_{(1)\text{ani, benz}}^{(3)}}$	$i_{HV}/i_{HV, \text{benz}}$
	$\lambda_a = 441.6 \text{ nm}$ $\lambda_b = \lambda_c = 694.3 \text{ nm}$	$\lambda_a = 632.8 \text{ nm}$ $\lambda_b = \lambda_c = 1064 \text{ nm}$	$\lambda_a = 530 \text{ nm}$ $\lambda_b = \lambda_c = 1064 \text{ nm}$	$\lambda_a = \lambda_b = \lambda_c = 546.1 \text{ nm}$	$\lambda_R = 546.1 \text{ nm}$
Benzene	1	1	1	1	1
Toluene	$1.3 \pm 0.3$	$1.4 \pm 0.3$		$1.3 \pm 0.3$	$1.31 \pm 0.01$
Mesitylene	$1.6 \pm 0.3$	$1.5 \pm 0.3$		$1.5 \pm 0.3$	$1.58 \pm 0.01$
Nitrobenzene		$5.3 \pm 0.8$		$5.6 \pm 0.8$	$6.18 \pm 0.06$
Carbon disulfide	$7.1 \pm 1.3$	$6.6 \pm 1.3$	$6.9 \pm 1.3$	$7.2 \pm 1.3$	$7.59 \pm 0.07$

Note. The dispersion with wavelength is performed according to Ref. 54.  $T = 293 \text{ K}$ . The nonlinear technique used here is OKE. The wavelengths  $\lambda_a, \lambda_b, \lambda_c$  refer to Eq. 4.



information on the spatial extent of these correlations, but also to study how this local order affects the spectrum of the scattered light. It is not the aim of this paper to give a detailed presentation of depolarized scattering of light. It can be shown that the normalized Rayleigh spectrum leads to  $g_2(\Delta\omega)$ , i.e., the Fourier transform of the  $l = 2$  spherical component of the spatially averaged orientation-dependent pair correlation function included in the expression of  $\gamma_{\text{eff}}^2$ . The simplest model of isotropic orientational diffusion predicts pure Lorentzian line shapes deriving from a purely exponentially decaying correlation function.

The associated relaxation time [29] is  $\tau_2 = \tau_D/3$  where  $\tau_D = 4\pi a^3 \eta / KT$ . In Debye's expression  $\eta$  is a shear viscosity and  $a$  the mean radius of the molecule, assumed to be spherical. In the case of asymmetric molecules,  $4\pi a^3$  can be replaced by  $kV$ , where  $V$  is the volume of the particle and  $k$  an empirical shape parameter that increases as the molecule becomes more elongated [46]. The main point here is that DRS exhibits the same characteristic time  $\tau_2$  as the one included in the denominator of the  $\chi_{1\text{ani}}^{(3)}$  expression (7). Then, direct comparison is allowed between the NLO investigations, performed in real time, and the studies of the frequency spectrum of DRS, generally recorded by spectrometric or interferometric methods. This method is used in this paper.

The relaxation time  $\tau_2$  is also an effective one, denoted  $\tau_{2,\text{eff}}$  which can be calculated from the spectral half-width at half-height (HWHH)  $\Delta\omega_{1/2}$  using the relation deduced from the Fourier transform:

$$\tau_{2,\text{eff}} = \frac{1}{2\pi \Delta\omega_{1/2}} \quad (14)$$

The exact link between  $\tau_{2,\text{eff}}$  and  $\tau_2$  is difficult to establish. It is generally assumed [46], in agreement with some experimental observations [55], that  $\tau_{2,\text{eff}} = (1 + J_A)\tau_2$  for symmetric top molecules,  $\tau_2$  being, as already noted, a linear function of shear viscosity.

### E. Relation Between Various Relaxation Times

The orientational motions of molecules in liquids and liquid crystals also contribute to many other physical effects. It will be interesting to compare the results obtained by these techniques to those obtained by NLO and DRS. For instance, these orientational motions give an important contribution to the broadening of nuclear magnetic resonance (NMR), far-infrared absorption (FIR), Raman scattering (RS), quasi-elastic neutron spectroscopy (QNS), and electron spin relaxation (ESR) lines. In all of these cases, comparisons between various components of the spatially

averaged function  $G(\Omega, t)$  already introduced will be possible and confrontation between the various characteristic times  $\tau_l$  ( $l$  is here the order of the corresponding Wigner function) are generally worthwhile. In the case of isotropic orientational diffusion of free particles, the various  $\tau_l$  are connected by the relation

$$\tau_l = 2\tau_D/l(l+1) \quad \text{where } l \neq 0 \quad (15)$$

An important case corresponds to  $l = 1$ .  $\tau_1 = \tau_D$  is then the dielectric decay time, obtained from dielectric relaxation (DR), and measured via the frequency dependence of the dielectric losses in the medium. In fact,  $\tau_{DR}$  is not directly equal to  $\tau_1$ , because of the response field of the surroundings to the permanent dipole  $\mu$  of the molecule, which can be important in liquid crystals [56]. Complete analysis given by Cole [57] leads to the relation

$$\tau_{DR} = \left( \frac{3\varepsilon_0}{2\varepsilon_0 + \varepsilon_\infty} \right) \tau_1 \quad (16)$$

where  $\varepsilon_0$  and  $\varepsilon_\infty$  are the dielectric constants taken, respectively, for  $\omega = 0$  and  $\omega \rightarrow \infty$  (optical régime). For 8CB,  $\varepsilon_0 \approx 6.0$  and  $\varepsilon_\infty = n^2 \approx 2.4$  lead to  $\tau_{DR} \approx 1.3\tau_1$ . One should also note that  $\tau_1 \sim 3\tau_2$ . Relaxation rates  $\tau_2 > 1$  ps correspond to dielectric frequencies up to 250 GHz, which are presently impossible to obtain and to use correctly.

The reader should not forget that the Brownian mechanism of orientational relaxation, which has been assumed in the previous analysis, has been found to be inappropriate in many instances, especially when short-range correlations exist. Many alternative jump models have been proposed, without any convincing proof of their adequacy to a true description of the real rotations in the liquids.

### III. NONLINEAR OPTICAL TECHNIQUES USED FOR THE STUDY OF FAST MOLECULAR RELAXATIONS IN LIQUID CRYSTALS

We restrict our presentation to techniques directly related to the third-order polarization  $\chi_{(1)}^{(3)}$ . However, we must mention the well-known technique of induced dichroism, developed in 1969 to study the effects of hydrogen bonding on orientational relaxation of laser dyes, such as rhodamine 6G [58, 59] and DODCI [60] and which is, at this time, used in our laboratory for the study of reorientation of dyes included in *Sm-A* liquid crystal films. A dichroism is induced by electronic excitation of molecules,

for instance, aligned along the picosecond pump linear polarization. The orientational distributional distribution of molecules in the ground state becomes anisotropic and the return to disorder can be investigated with the use of an absorbed auxiliary probe wave. We directly measure the sum  $(1/\tau_R + 1/\tau_F)$ , where  $\tau_R$  and  $\tau_F$  are respectively the orientational relaxation time and the characteristic time of decay of the excited species to the ground state. When  $\tau_F \gg \tau_R$ , direct investigation of molecular rotation is possible without any other measurement. Let us now present the principle of the three main techniques of NLO that have been used in the picosecond range.

### A. Optical Kerr Effect

The principle of the optical Kerr effect (OKE) is given in Fig. 2. It is described by putting  $\omega_A = \omega_{pr}$ ;  $\omega_b = -\omega_c = \omega_p$ ;  $\omega_\Sigma = \omega_{pr}$  in Eq. 8. In this case we obtain

$$\chi_{(1)\text{OKE}}^{(3)} = \frac{\rho}{45kT} \gamma(-\omega_{pr}, \omega_{pr}) \gamma(\omega_{pu}, -\omega_{pu}) \quad (17)$$

where  $\omega_{pr}$  and  $\omega_{pu}$  are respectively the frequencies of the probe and pump waves.

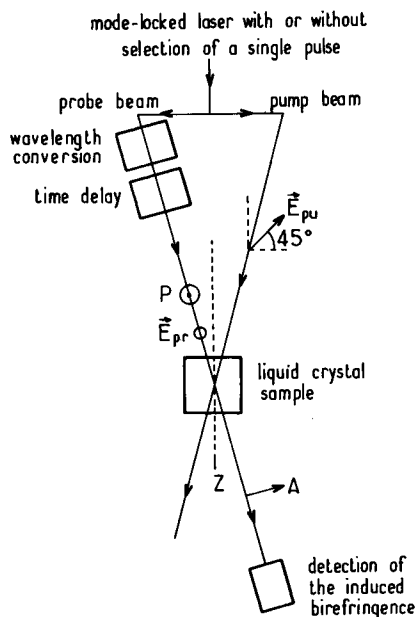


**Figure 2.** Principle of the OKE experiment; P and A are linear polarizations respectively perpendicular and parallel to the plane of the sheet.  $\vec{E}_{pu}$  is at 45° from this plane.

By using the relation

$$\Delta\varepsilon_{r,ij} - \delta_{ij} = \frac{1}{\varepsilon_0} \frac{P_{i(1)}^{(3)}}{E_j} \quad (18)$$

we can calculate the following expression of the refractive index increment  $\Delta n(\omega_{\text{pr}})$ , induced by the field  $|E_{\text{pu}}|$  of the pump, and analyzed by the probe:

$$\Delta n(\omega_{\text{pr}}) = \frac{\chi_{(1)\text{OKE}}^{(3)} |E_{\text{pu}}|^2}{30\varepsilon_0 n k T} = \lambda_{\text{pr}} B(\omega_{\text{pr}}, \omega_{\text{pu}}) |E_{\text{pu}}|^2 \quad (19)$$

where  $B$  is a temperature-dependent parameter describing OKE.

In the calculation of the transmission of the analyzing wave, convolution products between  $\Delta n(t)$  and the rectangular function of amplitude

$$\frac{n_{\text{pr}} n_{\text{pu}} z}{c} \left( \frac{1}{n_{\text{pu}}} \pm \frac{1}{n_{\text{pr}}} \right)$$

are used [61].  $z$  is the spatial coordinate of the traveling waves in the cell and  $c$  the speed of light.  $n_{\text{pr}}$  and  $n_{\text{pu}}$  are the mean values of the refractive indexes of the probe and pump waves;  $(-)$  is used when the two waves are propagating in the same direction, and  $(+)$  in the opposite case. Such a product is not adequate for thin films of liquid crystals. But for cells having some centimeters of thickness (such as the ones frequently used for the study of isotropic phases of liquid crystals) and optical waves of opposite directions, the width of the convolution product can reach values of about 100 ps, one or two orders of magnitude larger than the theoretical resolution of such an optical gate. In picosecond investigation, the probe and pump pulses must always be pointed in the same direction to avoid such a loss of time resolution. The pump light can be:

1. A high-repetition rate system, for instance, the wave given by passively or actively (or both) mode-locked dye or YAG lasers. The latter gives 25-ps pulses, which can be shortened to the picosecond range by time compression in monomode fibers. The use of cavity dumpers is often necessary to avoid accumulation effects due to the high frequency (about 100 MHz) of the delivered pulses.
2. A single pulse selected from a mode-locked laser train given by Nd/glass or Nd/YAG lasers. Techniques for achieving pulse selection have now reached an acceptable degree of reliability. Frequencies between 1 Hz and 1 kHz can be used.

The probe light can be:

1. A cw laser wave (He–Ne, He–Cd, or Ar and Kr lasers)
2. Second-harmonic pulses, delayed in time.

### B. Induced Transient Grating

The induced transient grating (ITG) principle is illustrated in Fig. 3. Samples are exposed to two picosecond excitation pump pulses, having the same wavelength but crossed linear polarizations. The two optical fields cannot interfere and thus do not give the usual intensity spatial modulation, which is known to generate the acoustic stationary waves that have recently been intensively studied. However, they add vectorially and create periodic variations of the orientation of molecules, giving rise to a phase modulation. Such an effect acts as a diffraction grating for a variably delayed probe. The changes in diffracted probe intensities as a function of time reflect the orientational processes within the sample. Generally, the detected signal comes from both the real and imaginary parts of the modulated complex refractive index. But, the effects due to the imaginary part are only important—as an induced dichroism—when both the pump and probe wavelengths lie within the absorption bands of the compounds, or when the laser intensity is high enough to induce two-photon absorption. In this case, the decay of the excited species can become important and can hide the orientational part of the signal. It is possible, however, to separate the different contributions by using variable polarizations of the waves [62]. With liquid crystal, wavelengths less than 400 nm must, for this reason, be systematically avoided. The polarization grating is located on equidistant planes, perpendicular to the vector:

$$\mathbf{K} = \mathbf{K}_{\text{pu},1} - \mathbf{K}_{\text{pu},2} \quad (20)$$

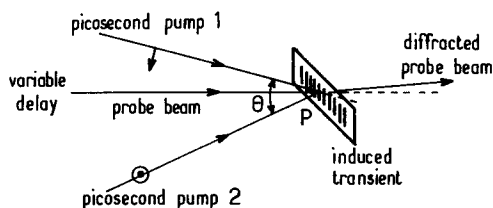


**Figure 3.** Principle of the ITG used for the measurement of molecular rotations. The two pump waves have crossed polarizations (horizontal and vertical). The polarization of the probe wave can be undetermined.

and separated by the spatial period:

$$\Lambda = 2\pi/|\mathbf{K}| = \lambda_{\text{pu}}/2 \sin(\theta/2) \quad (21)$$

where  $\theta$  is the angle ( $\mathbf{k}_{\text{pu},2}, \mathbf{k}_{\text{pu},2}$ ) and  $\lambda_{\text{pu}}$  the wavelength of the pump.

The distinction between thick and thin gratings, not too strongly modulated, can be made with the aid of the parameter  $Q$  defined as

$$Q = \frac{2\pi\lambda d}{n\Lambda^2} \quad (22)$$

where  $d$  is the thickness of the material and  $n$  its refractive index. With the typical values  $\lambda = 0.53 \mu\text{m}$ ,  $d_{\text{min}} = 250 \mu\text{m}$ ,  $n \approx 1.5$ , and  $\Lambda \approx 5 \mu\text{m}$ , we find  $Q \approx 20$ . We are in the case of thick grating. From a holographic treatment of [63], we know that only zero and first diffraction orders are present. As a result, high diffraction efficiency can be achieved. In this case, the diffraction efficiency  $\eta$  is given by

$$\eta = \frac{\sin^2\left(\nu\sqrt{1 + (\Delta k_z/2\nu)^2}\right)}{1 + (\Delta k_z/2\nu)^2} \quad (23)$$

with

$$\begin{aligned} \nu &= \pi \Delta n d / \lambda \cos \theta \\ \Delta k_z &= \frac{d}{\Lambda \cos \theta} (2\pi \sin \theta - \pi \lambda / n \Lambda) \end{aligned}$$

$\Delta n$  is the amplitude of the refractive index modulation and  $\theta$  the angle between the diffracted beam and the normal to the grating.

If the Bragg condition is fulfilled,  $\Delta k_z = 0$  and

$$\eta = \sin^2 \frac{\pi \Delta n d}{\lambda \cos \theta_B} \quad (24)$$

The maximum, ideally  $\eta = 1$ , is achieved for

$$\Delta n d = \frac{\lambda}{2} \cos \theta_B$$

with  $|k_i| = 2\pi n_i / \lambda_i$  and  $\theta_{\text{pr}}$ ,  $\theta_{\text{d}}$ ,  $\theta_{\text{pu},1}$  and  $\theta_{\text{pu},2}$ , respectively, the angles with the normal of the probe, diffracted, pump 1, and pump 2 waves is

fulfilled; i.e.,  $\Delta k_z = 0$ , the diffraction efficiency is highest. The maximum, ideally  $\nu = 1$ , is achieved for  $\nu_d = \pi/2$ . The intensity of the signal recorded versus time is basically related to  $\chi_{(1)\text{ani}}^{(3)}(-\omega_{\text{pr}}; \omega_{\text{pr}}; \omega_{\text{pu}}; -\omega_{\text{pu}})$  given by Eq. 7 and proportional to  $\Delta n^2(\omega_{\text{pr}})$  given by Eq. 20. The characteristic time is also  $\tau_2$ .

### C. Degenerate Four-Wave Mixing

The principle of degenerate four-wave mixing (DFWM) is illustrated in Fig. 4. In the DFWM, the sample is irradiated by two oppositely propagating pump waves (frequency  $\omega_L$ ; wave vectors  $\mathbf{k}_{\text{pu},1} = -\mathbf{k}_{\text{pu},2}$ ) and by a probe (frequency  $\omega_L$ ; wave vector  $\mathbf{k}_{\text{pr}}$ ) with a linear polarization perpendicular to that of the pumps. The angle  $(\mathbf{k}_{\text{pu},1}, \mathbf{k}_{\text{pr}})$  is about a few degrees. DFWM describes a process in which three input waves of the same frequency, but different propagation directions, mix and generate a fourth wave at the same frequency  $\omega_L$ . The time dependence of the process, induced with picosecond pulses, follows the decay of the pertinent material excitations, providing a way to study their dynamic behaviors. It is described by  $\chi_{(1)\text{ani}}^{(3)}(-\omega_L; \omega_L; \omega_L; -\omega_L)$  and directly linked to  $\gamma^2(-\omega_L; \omega_L)$ . We list here some of the most important features of this

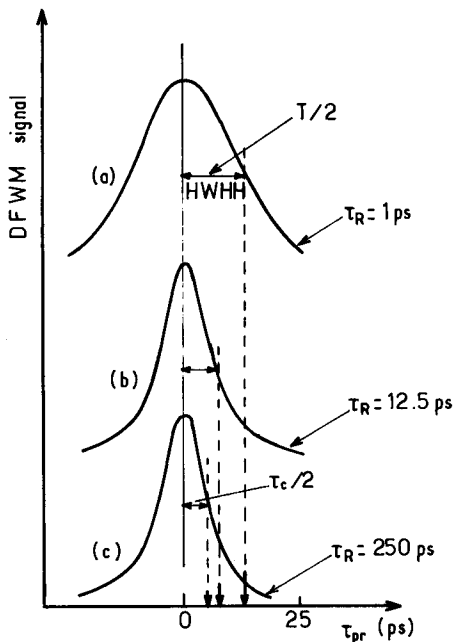


Figure 4. Computer calculation of the DFWM signal as a function of the probe time delay  $\tau_{\text{pr}}$  for three values of the reorientation time  $\tau_R$ . The pulse duration  $\tau$  and the coherence time  $\tau_c$  are held fixed at respectively 25 and 12.5 ps. (a)  $\tau_R \ll \tau$ ; (c)  $\tau_R \gg \tau$ ; (b) intermediate value of  $\tau_R$ .

effect, which have numerous applications:

- From a phase-matching consideration, it can be shown that the fourth wave has a conjugate phase of the probe and propagates in its reverse direction [28].
- DFWM is often described in terms of real-time holography [63]. As in ITG, two of the three incoming waves produce gratings. As already stated, any gratings built between pump 1 and pump 2 do not markedly contribute to the backward wave because of the phase mismatch in this direction. Pump 1 (respectively pump 2) and the probe produce polarization gratings of periods  $\Lambda_1$  and  $\Lambda_2$ , respectively, given by

$$\begin{aligned}\Lambda_1 &= \lambda/2 \sin(\theta/2) && \text{(pump 1-probe)} \\ \Lambda_2 &= \lambda/2 \cos(\theta/2) && \text{(pump 2-probe)}\end{aligned}\tag{25}$$

The angle  $\theta$  being small (a few degrees), we have  $\Lambda_1 \gg \Lambda_2$ . The DFWM signal is mainly due to the diffraction of pump 1 (respectively 2) by the phase grating produced by pump 2 (respectively 1) and probe, two waves having crossed polarizations. The analogy with ITG is obvious.

- $\gamma^2(-\omega_L, \omega_L)$  obtained with the DFWM technique does not suffer from the dispersion with frequencies, which affects both OKE and ITG and which can be important. Thus, DFWM and DRS lead to single-frequency determinations and can easily be performed at the same wavelength. This advantage should not be neglected.
- The most important advantages of DFWM lie in the fact that, besides the already mentioned conservation of linear momentum  $\hbar|\mathbf{k}|$  of the photons, the energy ( $\hbar\omega$ ) is also conserved, and the incident probe field is amplified simultaneously to the emission of intense backward waves. The sample behaves as a conjugate mirror with increased reflectivity [64]. This point is crucial because it allows the study of very thin samples (down to 50  $\mu\text{m}$ ) of well-oriented liquid crystal molecules, which cannot be studied by OKE, for which no coherent energy transfer occurs, and which need the use of thicker samples, if one want to avoid laser pulses that are too intense.
- As regards wave vector and phase, DFWM behaves like an ideal effect. For polarization, the situation appears to be more complicated [65]. In fact, the polarization of the backward wave should be deduced from the general laws of conservation of the angular momentum in a fixed quantization frame. It depends on the isotropic or anisotropic



character of the illuminated material. In the chosen geometry, the directions of polarization of the pumps and of the probe define the normal axes of the experiment, which remains unchanged during the nonlinear interaction in an isotropic medium. The result is that possible optical activity of samples does not play an important part in DFWM, while it can lead to a permanent, chirality-dependent, additional transparency in OKE.

A difficulty occurs in the NLO techniques when the duration  $\tau$  of the laser pulse (HWHH) is of the same order of magnitude as  $\tau_R = \tau_2$ , the relaxation time of the species. The usual solid-state lasers exhibit nonlinear optical behavior of their active material, leading to phase modulation of the pulses. Phase-modulated light pulses [66] are characterized by the coherence time  $\tau_c \approx 1/\Delta\nu$ , where  $\Delta\nu$  is the width of the pulse spectrum. For the different kinds of lasers used in this work, phase modulation is mainly due to the nonlinear refractive index of the glass or YAG rods and is known to be moderate (i.e.,  $0.5 \leq \tau_c \leq \tau$ , where  $\tau$  is the pulse duration;  $\Delta\nu$  is about 50 GHz). In this case, the pulse amplitude varies with time:

$$E(t) \approx \varepsilon(t) \exp[ia\varepsilon^2(t)]$$

where  $a \approx 2\tau/\tau_c$  measures the phase modulation, and  $\varepsilon(t)$  is given by

$$\varepsilon(t) = \exp[-2 \ln 2(t/\tau)^2] \quad (26)$$

When the reorientation time  $\tau_R$  is in the same range of values as  $\tau_c$ , which is the case in this work, the shape of the phase modulation is essential and the HWHH of the recorded signal as a function of the probe time delay  $\tau_{\text{pr}}$  is largely dependent on the ratio  $\tau_R/\tau$ .

Figure 5 gives computer simulations [67] of the recorded signals of ITG and DFWM, when there is no delay between the two pumps, in the three important cases  $\tau_R = 250$  ps,  $\tau_R = 12.5$  ps, and  $\tau_2 = 1$  ps. The value of  $\tau$  has been fixed at 25 ps (YAG laser pulse mean duration). The difference between the HWHH values are obvious: They allow one to estimate the relaxation time of nonlinear media. Such a method has already been used for the last few years and can be considered a useful supplement to the conventional pump-probe techniques, when the relaxation time to be measured is closed to the technical resolution limit. Results have been reported concerning crystalline silicon and liquids. Some of us have also studied oriented liquid crystals [67], but precise results can be obtained only in the two limiting cases  $\tau_c \approx \tau \ll \tau_R$  and  $\tau_c \approx \tau \gg \tau_R$ . Moreover, the results depend on the knowledge of the magnitude of the phase

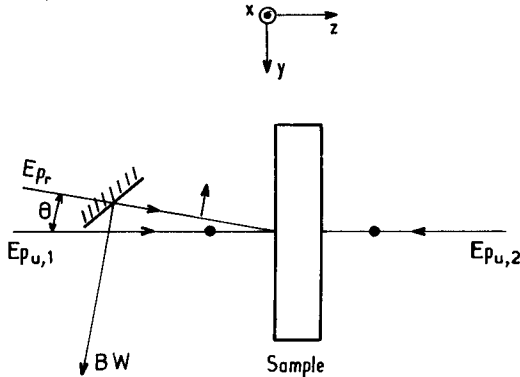


**Figure 5.** Principle of DFWM. The probe is linearly polarized in the plane of the figure. The two pumps have linear polarization perpendicular to the plane of the figure. BW, backward wave;  $\theta \approx 7^\circ$ .

modulation. We have preferred to avoid such difficulties in our DFWM experiments.

#### IV. THE LIQUID CRYSTALS AND THEIR PREPARATION

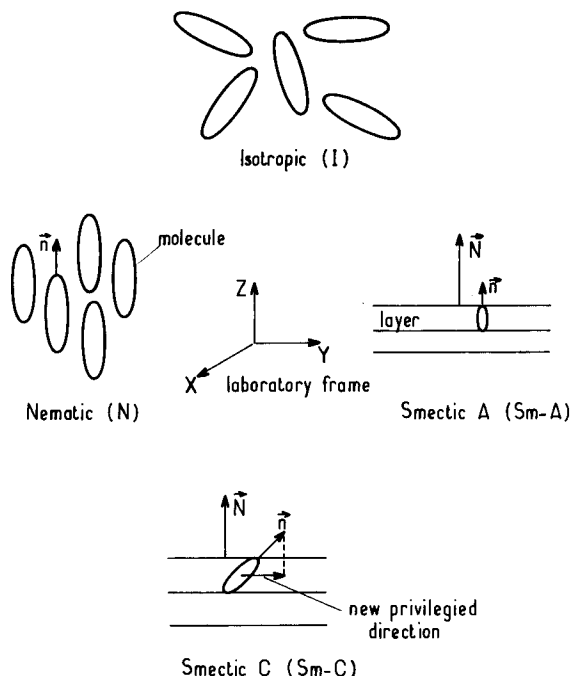
##### A. Structure of the Phases

An illustration of the molecular structure of isotropic ( $I$ ), nematic ( $N$ ) and smectic A and C ( $Sm-A$ ;  $Sm-C$ ) is given in Fig. 6.  $I$  phases are often considered as ordinary liquids. In fact, they exhibit rather complicated behavior. In  $N$  phases, there exists an orientational order only of the long molecular axis. This privileged direction is referred to by the unit vector  $\mathbf{n}$ , called the director of the phase. In  $Sm-A$  phases, an additional translational order leads to a layer structure characterized by the unit vector  $\mathbf{N}$  perpendicular to the layers. For  $Sm-A$  phases at rest,  $\mathbf{n}$  and  $\mathbf{N}$  are parallel to the  $Oz$  axis of the laboratory frame. Such a vision is highly idealized and fluctuations of both  $\mathbf{n}$  and  $\mathbf{N}$  occur in the two phases, due to all thermal, mechanical, and acoustical fluctuations in the samples. By lowering the temperature, one successively induces  $I \rightarrow N$ ;  $N \rightarrow Sm-A$ ;  $Sm-A \rightarrow Sm-C$  phase transitions. Some phases can be lacking in the classical sequence. By increasing the temperature, the opposite sequence is observed. Moreover, pretransitionnal behavior [1] exists in each phase. Near the phase-transition temperature, fluctuations develop in the high-temperature phase, giving rise to the local instantaneous order, which prefigures the order existing in the phase stable at lower temperature.

When chiral molecules are involved, the  $N$  phase is replaced by a cholesteric one,  $N^*$ , and original properties, due to a new helical order, are observed in the  $I^*$ ,  $Sm-A^*$ , and  $Sm-C^*$  phases. The most important of these new properties is ferroelectricity.

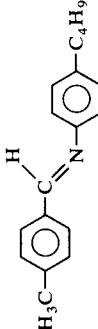
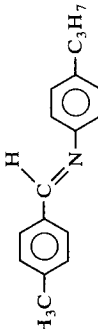
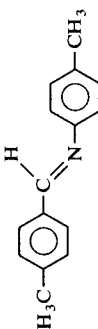

### B. The Compounds Studied

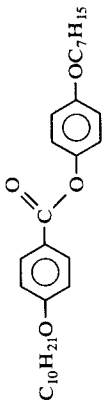
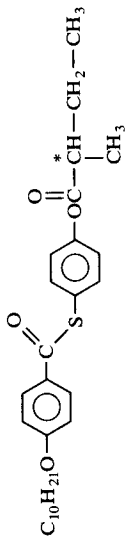
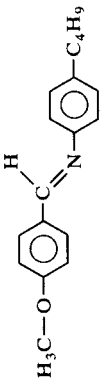
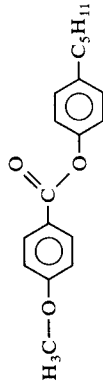
The nine compounds studied along with some of their principal physical properties are listed in Table III. Compounds 1–3 do not exhibit any stable thermotropic liquid crystal phases above their melting points. They can be considered as pseudo-nematogens in the temperature domain experimentally available. Compound 8 (MBBA) has a low chemical stability and its correct study remains difficult. All the other compounds can be studied without marked difficulty. Compounds 4, 5, 8, and 9 were purchased and used without further purification. The Merck mixture 5 has a compensated helical pitch in the  $N^*$  phase that diverges close to the  $Sm-A$  phase transition.



**Figure 6.** The structures of idealized isotropic ( $I$ ), nematic ( $N$ ), smectic-A ( $Sm-A$ ), and smectic-C ( $Sm-C$ ) phases at rest.

TABLE III  
The Studied Compounds and Some of Their Physical Properties

No. Compound	Origin	Molecular Formula	Chirality	Ferro- electricity	$T$ (°C)	
					$S_C \rightleftharpoons S_A$ or $S_C^* \rightleftharpoons S_A$	$S_A \rightleftharpoons N$ or $S_A \rightleftharpoons N^*$
1 MBA ( <i>p</i> -methyl- benzylidene- <i>p</i> ,' <i>n</i> '- butylaniline)	Home- synthesized		No	No	$S_A \rightleftharpoons N$ or $S_A \rightleftharpoons N^*$	$N \rightleftharpoons I$ or $N^* \rightleftharpoons I$
2 MPA ( <i>p</i> -methyl- benzylidene- <i>p</i> ,' <i>n</i> '- propylaniline)	Home- synthesized		No	No		
3 MMA ( <i>p</i> -methyl- benzylidene- <i>p</i> '- methylaniline)	Home- synthesized		No	No		
4 8CB ( <i>p</i> ,' <i>n</i> '-octyl- <i>p</i> '- cyanobiphenyl)	BDH		No	No	$S_A \rightleftharpoons N$ or $S_A \rightleftharpoons N^*$	33.5 40.8

5	ZLI 3488	Merck	Mixture unknown		Yes	61.0	66.0	85
6	4- <i>n</i> -Heptyloxyphenyl	Home-synthesized			No	83.2	87.1	90.6
7	4- <i>n</i> -Decyloxybenzoate-4-[2-methylbutanoyloxyphenyl]-4-decyloxythiobenzoate (racemic mixture)	Home-synthesized		Chiral by compensation	No	72.7	74.6	76
8	MBBA ( <i>p</i> -methoxybenzilidene- <i>p</i> , <i>n</i> -methylaniiline)	BDH			No			42.5
9	MBPB ( <i>p</i> -methoxybenzoate- <i>p</i> , <i>n</i> -pentybenzene)	Thomson			No			42.4

### C. Sample Preparation

From a general point of view, we must note that all the compounds studied were filtered through a pore size of  $0.1 \mu\text{m}$  to remove dust particles. All were warmed up to their clearing points to eliminate all gas bubbles, which would exist in high-viscosity phases (*Sm-A*, for instance). All the cells were glass cells, always used without any adhesive or elastomer, and were housed in temperature-controlled ovens with a nominal temperature stability of  $0.01^\circ\text{C}$ . In the studies of OKE in isotropic phases (*I*), cells in the range of the centimeter range were used. For oriented phases, two thicknesses, 200 and  $500 \mu\text{m}$ , were used. The most difficult problem is obtaining samples of high optical quality with a good alignment of particles. The reported work concerns homeotropic alignment in the nematic (*N*) and smectic A (*Sm-A*) phases. In such an alignment, the director  $\mathbf{n}$  of the phase (along the *Oz* axis; see Fig. 6) is perpendicular to the faces of the cells (*xOy* plane). This was obtained by coating the inner faces of the windows of the cell with octadecyl triethoxysilane in propanol-2 solution. A partial polymerization of the product was performed by heating the coating at  $120^\circ\text{C}$  for 1 h. The cell was filled with the compound in the *I* phase. Then, the temperature was slowly decreased to the *Sm-A* phase in a few hours. The alignment can be greatly improved with static magnetic inductions perpendicular to the surfaces. Two magnets of about 3000 g and 10 000 g were used. The orientation of molecules occurs in the *N* phase. When it does not exist, orientation can be obtained at the  $I \rightleftharpoons Sm-A$  phase transition by using the highest induction. For the Merck mixture 5, alignment can be obtained only at the  $N^* \rightleftharpoons Sm-A$  phase transition, where the pitch diverges. One must note that there is no helical pitch in the classical *Sm-A*\* phases of our studies, except in the vicinity of the  $Sm-A^* \rightleftharpoons Sm-C^*$  phase transition, where, as previously mentioned, pretransitional order can occur (the *Sm-C*\* phase has a helical structure).

### D. Control of the Optical Quality of the Samples

The *Sm-C* and *Sm-C*\* phases of the compounds in this experiment are opaque and cannot be studied. All the other phases are transparent and look like glass. They must be free from dust and bubbles when observed with a magnifying lens (*I* phases). For *N* and *Sm-A* phases, two additional steps were performed: First, the alignment was readily verified by observing the characteristic dark cross in the conoscopic pattern under a polarizing microscope using focused light. Then, the extinction ratio was measured with parallel light, between crossed polarizers both normal to the wave vector of the light and to the director of the phase. Typical values

of about  $1/3000$  were obtained for  $Sm-A$  phases. Samples were rejected if the ratio was higher than  $1/1000$ . For  $Sm-A$  phases, we also verified that optical activity does not play an important part in the DFWM experiment. For  $500\text{-}\mu\text{m}$  thickness, rotations less than some minutes of the arc were measured, far from the  $Sm-A \rightleftharpoons Sm-C^*$  phase transition, in agreement with other investigations [68, 69].

The optical quality of the sample governs its behavior in the applied high-power light pulses. The laser intensity is always adjusted, using glass filters, to values where laser-induced dielectric breakdown within the sample occurs very infrequently. For all the liquid crystals studied, the refuse produced by a single breakdown would reduce the dielectric strength of the sample enough to necessitate its change. Moreover, when it accidentally occurs, visible damage is observed on the sample or on the windows of the cell. Typically, the laser has to be attenuated to less than  $0.1$  MW to prevent breakdown. In OKE experiments, we do not focus the pump and probe waves. In DFWM experiments, lenses of long focal lengths (some tens of centimeters) are used, not to focus the waves, but to slightly reduce their diameters.

## V. EXPERIMENTS AND RESULTS

### A. OKE Investigations

As previously noted, the laser-induced refractive index increment  $\Delta n_{\text{OKE}}$  is proportional to the OKE constant  $B$  (Eq. (19)), which basically varies as the length  $l$  of the sample. The OKE signal varies as  $l^2$  and it is difficult to detect reliable OKE signals with samples of some hundreds of micrometers such as the ones containing oriented  $N$  or  $Sm-A$  phases. Thus, the reported OKE investigations concern only  $I$  phases.

#### 1. *Studies of Slow Responses to Picosecond Pulses [12]*

*a. Methods and Materials.* The experimental setup is shown in Fig. 7. The pump wave was provided by a home-made passively mode-locked  $\text{Nd}^{3+}$ /glass laser. The dye used was the Eastman Kodak 9740 solution housed in a cell,  $100\ \mu\text{m}$  thick, placed inside an afocal optical (diverging lens-concave mirror  $R = 5\ \text{m}$ ) system constituting the rear reflector of the cavity. This allowed us to reduce the energy density inside the dye solution and thus to increase its lifetime. The cavity round-trip was about  $6\ \text{ns}$ . Pulse selection was performed by a home-made electronic shutter driven by the mode-locked oscillator. An amplifier (gain about 30) increased the

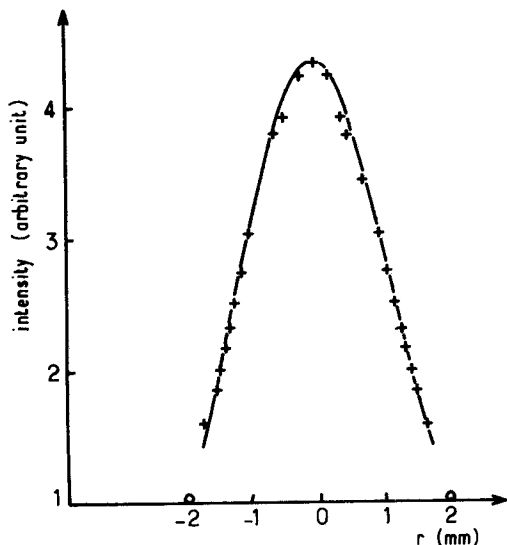


**Figure 7.** Experimental setup.  $P_1$ ,  $P_3$ , Glan prism;  $P_2$ , Wollaston prism;  $D_1$ , CSF CPA 1443 photodiode;  $D_2$ , Hewlett-Packard 5082-4207 photodiode;  $PM_1$ , La Radiotechnique 150 CVD photomultiplier;  $PM_2$ , La Radiotechnique XP 2018 photomultiplier;  $L$ , beamsplitters; the pump laser is a single pulse  $Nd^{3+}$ /glass laser; the cw probing laser can be He-Ne or He-Cd Spectra Physics models 125 or 185.

energy of a single pulse up to a few millijoules. Of course, the transverse structure of the inducing wave must be highly reproducible. The amplitude of the OKE signal appears to be proportional to

$$\left[ \int_x \int_y [E_{pu}^2(x, y) E_{2pr}(x, y) dx dy]^2, \right.$$

where  $(x, y)$  are the coordinates in a plane perpendicular to the common direction of the wavevectors of both pump and probe. Usually,  $E_{pr}(x, y)$  corresponds to the  $TEM_{00}$  mode of a gas laser and has a good time range stability. Thus, a simple condition for keeping the value of the last expression constant is to use a pump laser oscillating on the  $TEM_{00}$  mode. The mode selection was obtained by inserting a pinhole with 2.0-mm diameter into the laser cavity. Figure 8 shows the transverse structure of the 1064-nm pump laser recorded near the sample. As a consequence of Fresnel diffraction, the structure was expected to become nearly Gaussian at some distance from the laser. The fit of the experimental results by a



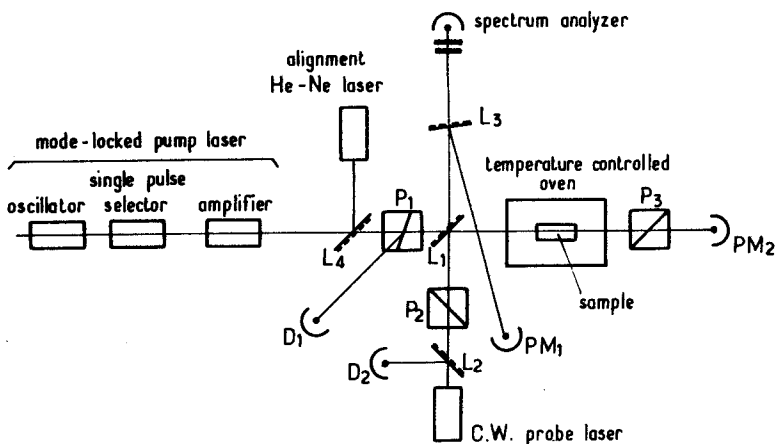


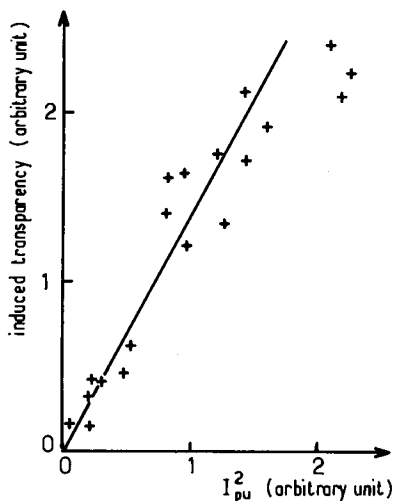
**Figure 8.** Gaussian distribution of the energy of the pump laser versus radial distance to the axis. The detection photodiode was placed near the sample. +, experimental points; -, fit of experimental results to  $\exp(-r^2/a^2)$ .  $a$  was kept free during the fit.

Gaussian distribution seems to be good. The divergence is near  $\Delta\theta \approx 6 \times 10^{-4}$  rad, corresponding to the theoretical value of the far-field divergence of a fundamental mode of  $560\text{-}\mu\text{m}$  beam waist ( $\gamma_0 = \lambda_{\text{pu}}/\pi \Delta\theta$ ).

The natural complement to the study of transverse structure of the pump wave is the study of its time duration. We measured  $\tau_{\text{pu}}$  with a two-photon fluorescence method performed on the single pulse and found  $\tau_{\text{pu}} = (7 \pm 1)$  ps. The pump wave was linearly polarized by the Brewster cut of the active rod and by the Glan prism  $P_1$  at  $45^\circ$  to the vertical. The reflected part of the pump was sampled by a fast photodiode which triggered the oscilloscope. The energy of the pump pulse was measured by a photomultiplier coupled to a photon-coupling device.

For probe waves we used both single-mode He-Ne ( $\lambda_{\text{pr}} = 632$  nm) and He-Cd ( $\lambda_{\text{pr}} = 441.6$  nm) lasers (mean powers of a few milliwatts). The intensity of the probe during the pump action in the sample was measured by means of a pin photodiode coupled with a storage oscilloscope. The probe was linearly and vertically polarized by a Wollaston prism, carefully crossed with the Glan prism placed after the cell.

Detection of the OKE signal was performed by a fast photomultiplier. We measured its impulse response by using pulses of less than 1-ns duration delivered by a flash generator. The response is then quasi-symmetrical with no trailing tail. The rise time and the FWHH were, respectively, 1.5 and 2.4 ns. The photomultiplier was directly connected to a 500-MHz digitizer.



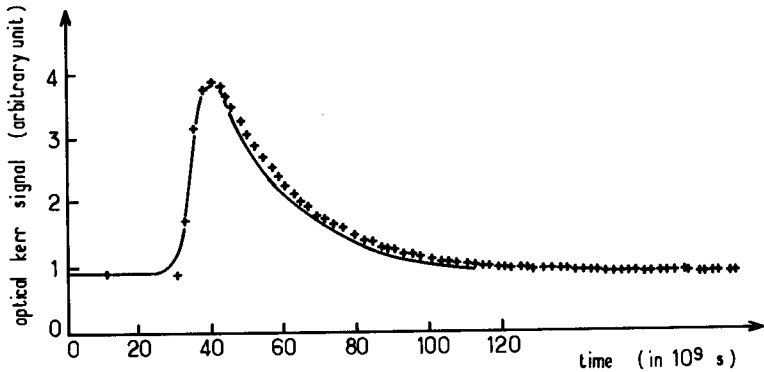
**Figure 9.** Variations of the induced transparency  $\tau$  versus  $I_{pu}^2$ . +, experimental points; -, linear dependence for weak values of  $I_{pu}^2$ ; compound: MBPB at  $45.00 \pm 0.01^\circ\text{C}$ ;  $\lambda_{pr} = 632.8$  nm; length of the cell: 4 cm.

Figure 9 shows the variations of the OKE signal (which is proportional to  $\sin^2(\Delta\psi/2)$ , where  $\Delta\psi$  is the phase change in the cell) versus  $I_{pu}^2 \propto E_{pu}^4$ . The variation of the phase is easily related to  $\Delta n_{OKE}$  and  $B$  by

$$\Delta\psi = \frac{2\pi \Delta n_{OKE}}{\lambda_{pr}} = 2\pi l B E_{pu}^2 \quad (27)$$

where  $l$  is the length of the cell. We see that, for the highest values of  $I_{pu}$ , the signal measured is no longer proportional to  $I_{pu}^2$ . We may assume that, in this case,  $\sin^2 \Delta\psi/2$  can no longer be approximated by  $\Delta\psi^2/4$ . In fact, the observed divergence can also be attributed to a self-focusing effect [70]. We shall not discuss here the numerous and complex mechanisms responsible for this effect. As is well known, in the picosecond range and in the case of liquids with large values of OKE constants, molecular reorientation plays the main role [71]. Correlatively, parasitic nonlinear effects (Raman and Brillouin stimulated effects, for instance) are generated in the sample and can dissipate an important part of the pump energy. We do not try to estimate the relative importance of these two contributions and we make an effort to perform the experiment with the lowest intensity of the pump, for which the OKE signal is always linear in  $I_{pu}^2$ .

*b. Results.* Compounds 8 and 9 were studied. In Fig. 10 we show an example of an OKE signal recorded versus time at fixed temperature for



**Figure 10.** Variations of OKE signal versus time.  $\tau_{pu} = 7 \pm 1$  ps;  $\lambda_{pr} = 632.8$  nm; compound: MBPB at  $(50.00 \pm 0.02)^\circ\text{C}$ ; length of the cell: 30 cm; -, experimental oscilloscope trace; ···, fit of results to Eq. 42.

the compound MBPB in its isotropic phase. The rise time is in the nanosecond range, i.e., of the same order as the rise time of the photomultiplier that records the signal. The relaxation of the birefringence is in the  $10^{-8}$ -s range. A logarithmic plot (not reported here) is in favor of a pure exponential relaxation with a characteristic time  $\tau_R$ . Obviously, such a relaxation time is two or three orders of magnitude larger than the one expected from pure molecular reorientation. The Landau-de Gennes theory [72, 73] of the isotropic-nematic phase transition can be successfully used for the description of the observed relaxation. As we have noted, the nematic phase of a liquid crystal is composed of anisotropic particles having their long axis nearly parallel to the director  $\mathbf{n}$  and their centers of mass randomly distributed. Macroscopically, the medium is uniaxial, but the molecular permanent electrical dipoles are rather uncoupled and the symmetry of the phase is quadrupolar, with a microscopic order parameter describing the orientational correlations between the long axes given by

$$Q_{ij} = \frac{1}{2}S(n_i n_j - \delta_{ij}) \quad (28)$$

Here  $n_i$  is the component of the local optical axis  $\mathbf{n}$  along the direction  $\mathbf{i}$  of the laboratory frame,  $S$  is a scalar order parameter, and  $Q_{ij}$  is a traceless second-order tensor. If  $\theta$  denotes the angle between  $\mathbf{n}$  and the direction of the long axis, then  $S$  can be written in the form

$$S = \frac{1}{2}\langle 3 \cos^2 \theta - 1 \rangle$$

Beyond  $T_{\text{NI}}$ , the value of  $S$  decreases to zero discontinuously and the sample becomes macroscopically isotropic ( $I$  phase). In the  $I$  phase, when  $T$  decreases toward  $T_{\text{NI}}$ , pretransitional nematic order develops, leading to fluctuations characterized by a lifetime  $\tau$  and a geometrical extension measured by the correlation length  $\xi$ .

Let us now briefly recall the de Gennes theory. The free energy per unit volume  $F$  is expanded as a power function of the order parameter (the elastic terms have been omitted):

$$F = F_0 + \frac{1}{2}AQ_{ij}Q_{ij} - \frac{1}{3}BQ_{ij}Q_{jk}Q_{ki} + \frac{1}{4}CQ_{ij}Q_{jk}Q_{kl}Q_{li} - \frac{1}{2}\chi_{ij}E_iE_j + \dots \quad (29)$$

where  $E$  is a field and  $\chi_{ij}$  is the corresponding susceptibility.  $Q_{ij}$  is a new order parameter, defined from macroscopic data only and such that

$$Q_{ij} = \frac{3}{2\Delta\chi} \left( \chi_{ij} - \frac{1}{3}\chi_{kk}\delta_{ij} \right) \quad (30)$$

Here  $\Delta\chi = (\chi_{\parallel} - \chi_{\perp})$ , where  $\chi_{\parallel}$  and  $\chi_{\perp}$  refer to a perfectly aligned medium with  $S = 1$ . The coefficient  $A$  is assumed to vary with temperature:

$$A = a(T - T_c)^\alpha \quad \alpha > 0 \quad (31)$$

The NI transition occurs at  $T_{\text{NI}}$  slightly above  $T_c$ , given by

$$A = a(T_{\text{NI}} - T_c)^\alpha = 2B^2/27C \quad (32)$$

At  $T_{\text{NI}}$ ,  $S$  jumps from 0 to  $2B/9C$ . According to the thermodynamics of irreversible processes, we can define a viscosity  $\eta$  by

$$\eta\dot{Q}_{ij} = -\frac{\partial F}{\partial Q_{ij}} \quad (33)$$

We have neglected the coupling between  $Q_{ij}$  and the velocity gradients by assuming the absence of flow constraint in the sample.

Taking into account only the first term in the right-hand part of Eq. (29), we can write

$$\eta\dot{Q}_{ij} \neq -AQ_{ij} + \frac{1}{2}\Delta\chi_{\omega_{\text{pu}}}(E_iE_j - \frac{1}{3}E^2\delta_{ij}) \quad (34)$$

where  $\Delta\chi(\omega_{\text{pu}})$  is related to the optical Kerr constant  $B(\omega_{\text{pu}}, \omega_{\text{pr}})$  and to the refractive index  $n(\omega_{\text{pr}})$  at frequency  $\omega_{\text{pr}}$  and wavelength  $\lambda_{\text{pr}}$  of the probe wave by

$$B(\omega_{\text{pr}}, \omega_{\text{pu}}) = \frac{\Delta\chi(\omega_{\text{pr}})\Delta\chi(\omega_{\text{pu}})}{4\epsilon n(\omega_{\text{pr}})\lambda_{\text{pr}}A} \quad (35)$$

with  $A = a(T - T_c)^\alpha$  (Eq. 32). The OKE constant varies as  $A^{-1}$ , i.e., as  $1/(T - T_c)^\alpha$ .

The theoretical prediction of the value of  $\alpha$  requires a microscopic description of the system, allowing the calculation of the angular correlation parameter  $J_A$  (Eq. (13)). The link with the phenomenological theory is then ensured by the microscopic expression of the OKE constant:

$$B(\omega_{\text{pr}}, \omega_{\text{pu}}) \propto \gamma(-\omega_{\text{pr}}, \omega_{\text{pr}})\gamma(-\omega_{\text{pu}}, \omega_{\text{pu}})(1 + J_A) \quad (36)$$

Let us recall here that mean-field theory [74] leads to  $(1 + J_A) \propto 1/(T - T_c)$ , that is,  $\alpha = 1$ . It is now possible, from Eq. (35), to calculate the phase variation  $\Delta\varphi$  induced at time  $t$  and length  $l$ . We find

$$\Delta\varphi = \frac{2\pi}{\lambda_{\text{pr}}} \int_0^l \Delta n(z, t) dz \quad (37)$$

with

$$\Delta n(z, t) = B(\omega_{\text{pr}}, \omega_{\text{pu}})\lambda_{\text{pr}} \int_{-\infty}^t E_{\text{pu}}^2(z, t') f(t - t') dt' \quad (38)$$

$f(t)$  is given by integration of Eq. (34) and appears as a pure exponential relaxation which can be written for positive times:

$$f_1(t) = \frac{1}{\tau_R} \exp\left(\frac{-t}{\tau_R}\right) \quad (39)$$

where  $\tau_R = \eta/a(T - T_c)^\alpha$ .

Because the orientational relaxation times involved here are at least of the order of several nanoseconds, one may neglect the group mismatch [75] between pump and probe. Moreover, the time dependent of  $E_{\text{pu}}^2$  will be approximated by a Dirac pulse. Thus,

$$E_{\text{pu}}^2(z, t') = I_{\text{pu}} e^{-\alpha_{\text{pu}} z} \delta(t')$$

where  $I_{\text{pu}} = \int_{-\infty}^{+\infty} E_{\text{pu}}^2 dt$  is the energy of the pump pulse. Equation (38) becomes

$$\Delta n(z, t) = \frac{B(\omega_{\text{pr}}, \omega_{\text{pu}}) \lambda_{\text{pu}} I_{\text{pu}} e^{-\alpha_{\text{pu}} z}}{\tau_{\text{R}}} Y(t) \exp\left(\frac{-t}{\tau_{\text{R}}}\right) \quad (40)$$

Then, putting this result in Eq. (37), we find

$$\Delta\varphi = \frac{2\pi B(\omega_{\text{pr}}, \omega_{\text{pu}}) I_{\text{pu}} [1 - \exp(-\alpha_{\text{pl}} l)]}{\alpha_{\text{pu}} \tau_{\text{R}}} Y(t) \exp\left(\frac{-t}{\tau_{\text{R}}}\right) \quad (41)$$

where  $Y(t) = 1$  for  $t > 0$  and  $Y(t) = 0$  for  $t < 0$ .

The OKE signal is proportional to

$$\mathcal{I} = \exp(-\alpha_{\text{pr}} l) \sin^2 \frac{\Delta\varphi}{2} \approx \frac{1}{4} \exp(-\alpha_{\text{pr}} l) \Delta\varphi^2$$

where  $\alpha_{\text{pr}}$  is the absorption rate of the probe assumed to be polarization independent.  $\mathcal{I}$  will be called induced transparency. The OKE signal decreases when  $\tau_{\text{R}}$  increases as  $1/\tau_{\text{R}}^2$ . We must observe a pure exponential decay with a time constant  $\tau_{\text{R}}/2$ . Figure 11 shows the experimental results [76] obtained with MBPB—taking into account the response time

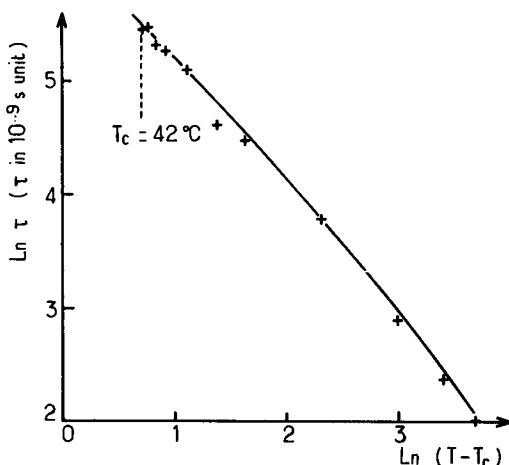


**Figure 11.** Variations of  $\tau_{\text{R}}$  with  $\ln(T - T_c)$ . Compound: MBPB; length of the cell: 30 cm;  $\tau_{\text{pu}}$ :  $7 \pm 1$  ps;  $\lambda_{\text{pr}} = 632.8$  nm; +, experimental values; -, fit to Eq. 42.

TABLE IV  
Absorption Rate of MBPB at the Three Wavelengths Used

		$\lambda = 632.8 \text{ nm}$									
$T$ ( $^{\circ}\text{C}$ )	42	42.2	42.4	42.6	42.8	43	44	45	50	57	65
$\alpha$ ( $\text{m}^{-1}$ )	4.38	4.08	3.45	2.93	2.70	2.68	1.74	1.44	1.40	1.11	0.14
		$\lambda = 441.6 \text{ nm}$									
$T$ ( $^{\circ}\text{C}$ )	42.10	42.31	42.72	43.12	44.20	45.06	47.15	49.11	51.19	53.16	57.11
$\alpha$ ( $\text{m}^{-1}$ )	32.10	24.0	14.78	12.08	7.58	7.58	3.40	3.56	3.20	2.40	2.02
		$\lambda = 1060 \text{ nm}$									
$T$ ( $^{\circ}\text{C}$ )	42	42.2	42.4	42.6	42.8	43	44	45	50	57	62
$\alpha$ ( $\text{m}^{-1}$ )	3.48	3.48	3.48	3.48	3.17	3.17	2.86	2.25	1.65	1.36	0.79

of the photomultiplier used for detection—and its fit to Eq. (41). Agreement is good and confirms the single relaxation expected. This has also been observed for all other temperatures checked. The relaxation times vary from about 7 ns (at  $38^{\circ}$  above the  $I \rightleftharpoons N$  phase transition) to 230 ns at the phase transition temperature. In these experiments, a 632.8-nm probe wavelength was used. Quite the same results have been observed by probing at 441.6 nm, i.e., for a wave with an 8 times greater absorption coefficient. Table IV gives the measured absorption coefficients at the three wavelengths used. Their variations with temperature appear to be important.

The identity of the observed behaviors being the proof that the probe wave does not induce any appreciable thermal effects in the long cells (many centimeters) used here. A quantitative comparison with de Gennes behavior is presented in Fig. 12. The results have been fit to the relation

$$\tau_R = \eta/a(T - T_c) \quad (42)$$

by assuming a temperature dependence of the viscosity coefficient  $\eta$  of the type  $\eta = \eta_0 \exp(T_0/T)$  (where  $\eta_0$  and  $T_0$  are constants) and putting  $\alpha = 1$ , as predicted by mean-field theory. The agreement is good, leading to values of  $T_0 \neq 1475 \text{ K}$  and  $T_c \neq 40.0^{\circ}\text{C}$ . The same results were obtained with MBBA. They confirm older results obtained with  $Q$ -switched laser pulses in the range of about 10 ns, a duration that cannot be neglected when compared to the relaxation time of the sample.

Let us now discuss the variations of the parameter  $B$  with temperature. Equation (36) shows that  $B^{-1}(\omega_{pr}, \omega_{pu})$  varies as  $(T - T_c)^\alpha$ . We have shown that  $\alpha \neq 1$ . Then  $B^{-1}(\omega_{pr}, \omega_{pu})$  must exhibit a linear variation with

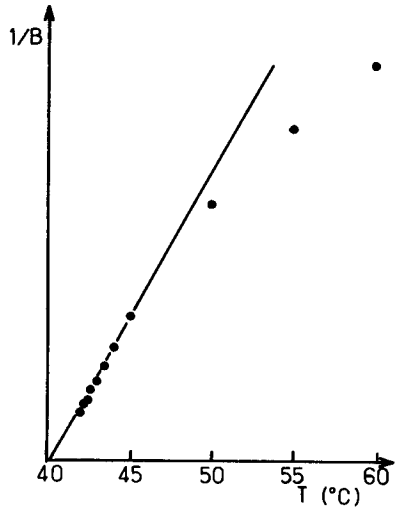


**Figure 12.** Variations of  $B^{-1}$  versus  $T$ . Compound: MBPB; length of the cell: 4 cm;  $\tau_{pu} \approx 30$  ns;  $\lambda_{pr} = 441.6$  nm; ●, experimental points; —, linear dependence in the vicinity of  $T_{NI}$ .

temperature. This linear behavior was first observed by Shen et al. [77, 78] about twenty years ago. During the same period we observed, for many compounds, nonlinear thermal behavior [74]. Figure 13 shows results obtained with MBPB, and nanosecond pulse excitation, where what we observe is an increasing departure from the linear behavior for high temperatures, i.e., far from the  $N \rightleftharpoons I$  phase transition. Such an anomaly was also reported in some Cotton–Mouton and Kerr effects investigations [80, 81]. Our investigations led to the conclusion that a  $(T - T_c)^{-1}$ -type law is obeyed only if  $(T - T_c)$  is less than about  $10^\circ$ . At higher temperatures, the decrease of  $B$  is slower than predicted by the mean-field law. An explanation can be found if we keep in mind that, till now, the theoretical background chosen has been that of the  $I \rightleftharpoons N$  phase transition.

We have assumed that the fluctuations of the order parameter, characteristic of the phase transition are the only relevant mechanism describing the response of the system to the optical field. Such a simplification appears to be relevant in the vicinity of the transition temperature, where these fluctuations are large enough to hide any other noncritical mechanism. When the temperature increases, the fluctuations of the macroscopic order parameter and, consequently, the nematogenic character of the liquid, decrease drastically. Thus, we may expect its behavior to approach that of ordinary liquids; that is, a supplementary noncritical contribution should appear at high temperatures. In Fig. 14,  $B$  is plotted vs.  $(T - T_c)^{-1}$ , with the value of  $T_c$  taken from the previously described relaxation



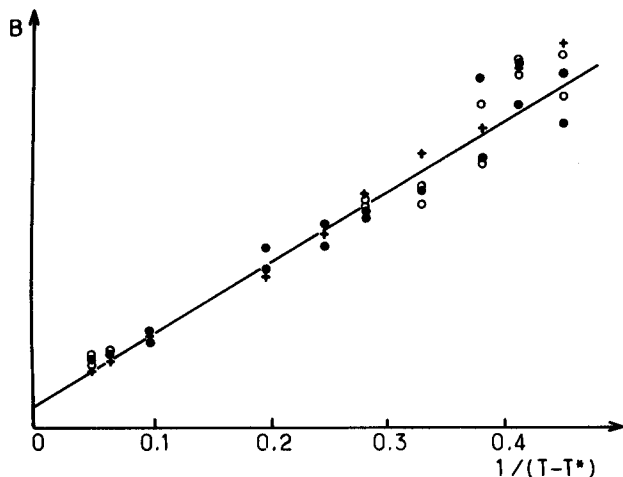


**Figure 13.** Variations of  $B$  versus  $1/T - T^*$ . Compound: MBPB; length of the cell: 4 cm;  $\tau_{pu} \approx 30$  ns;  $\lambda_{pr} = 632.8$  nm;  $\bullet$ ,  $+$ ,  $\circ$ : experimental points corresponding to three different methods of evaluation of  $B$  (see Ref. 76);  $-$ , fit to Eq. 44. During the fit, the value  $T_c = 40.0^\circ\text{C}$  (obtained from independent relaxation data) was held fixed.

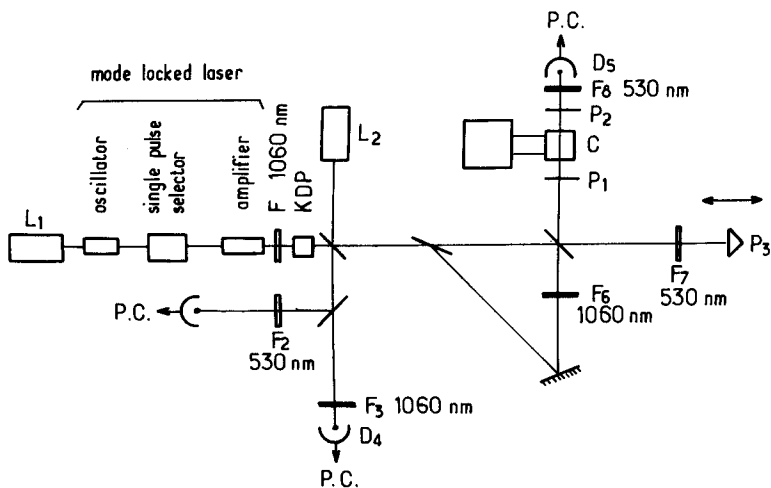


**Figure 14.** Experimental arrangement.  $L_1$ ,  $L_2$ ; He-Ne lasers; F, interference filters;  $P_1$ ,  $P_2$ , HN22 polaroid;  $P_3$ , prism; D, photomultipliers associated to photon-counting devices; C, sample in its oven.

studies. The graph seems effectively well fitted by the function

$$B = B_1 + B_2 = \frac{b}{(T - T_c)} + \frac{b'}{T} \quad (43)$$

where  $B_1$  is the contribution related to de Gennes' theory in the mean-field approximation, while  $B_2$  appears to be a smoothly varying contribution. This additional contribution must also be included in a correct treatment of a depolarized Rayleigh scattering experiment performed in MBBA [76]. Of course, the additional contribution is expected to relax much more quickly than the "cooperative" one of the order parameter. It is quite impossible to detect it in the OKE relaxation presented in Fig. 11. We therefore decided to use a more appropriate approach in our OKE investigations.

## 2. Studies of Fast Responses in OKE Investigations [14, 15]

*a. Methods and Materials.* The experimental setup is shown in Fig. 14. The OKE is induced by the  $\lambda_{\text{pu}} = 1060$  nm,  $\tau_{\text{pu}} = (7 \pm 1)$ -ps pulses given by the  $\text{Nd}^{3+}$ /glass laser previously described, with a linear polarization at  $45^\circ$  to the optical axes, respectively horizontal and vertical of the polarizers  $P_1$  and  $P_2$ . Green pulses at 530 nm were generated by second-harmonic generation (SHG) in a KDP crystal, slightly mistuned to reduce the conversion and giving linear horizontal polarization. The green pulses were used to probe the induced birefringence created by the infrared pump pulses in the sample. We measured the duration  $\tau_{\text{pr}}$  of these pulses using classical techniques of NLO [15] and found  $\tau_{\text{pr}} = (5 \pm 1)$  ps.

The probe pulses can be continuously delayed in time with respect to the pump pulses, up to a value of 5 ns and with an uncertainty not larger than 1 ps, by varying the position of the prism PR. At each fixed position of PR, photomultipliers associated with photon counting techniques simultaneously measured the energies of the pump, the probe, and the OKE pulses. We controlled both the dependence of the signal with  $I_{\text{pu}}^2$  and the linear transmission of the sample with  $I_{\text{pr}}$  (absence of nonlinear effects on the probe).

As we mentioned, the pump and probe pulses propagated in the same direction to avoid a loss of time resolution during the investigations. An example of the recorded signal is given in Fig. 15. As expected from previous discussion, fast relaxation can be observed, associated with slower relaxation.

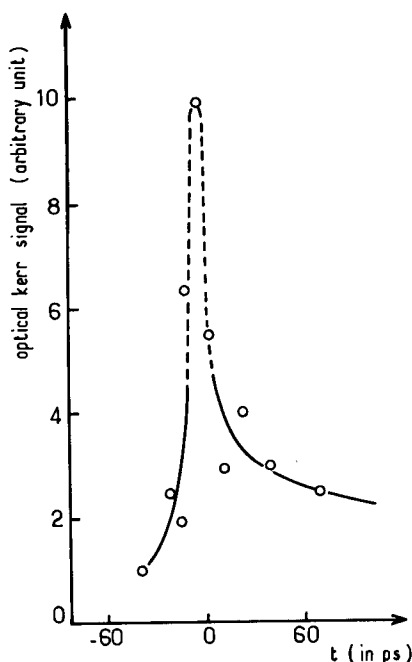


Figure 15. Example of OKE signal obtained with MPBP;  $(50.00 \pm 0.00)^\circ\text{C}$ .

Let us assume the presence of two relaxations, fast (F) and slow (S). The response function must now be written

$$f_2(t) = \frac{C_S}{\tau_{R,S}} \exp\left(-\frac{t}{\tau_{R,S}}\right) + \frac{C_F}{\tau_{R,F}} \exp\left(-\frac{t}{\tau_{R,F}}\right) \quad (44)$$

The transient birefringence induced at time  $t$  and coordinate  $z$  along the axis of the sample is given by

$$\Delta n(z, t) = B\lambda_{\text{pr}} \int_{-\infty}^t f_2(t-t') E_{\text{pu}}^2(z, t') dt' \quad (45)$$

By assuming Gaussian time distributions for the pulses

$$I_{\text{pu}}(z, t) = I_{\text{pu},0} \exp\left[-\frac{(t - n_{\text{pu}}z/c)^2}{\tau_{\text{pu}}^2}\right] \quad (46)$$

$$I_{\text{pr}}(z, t) = I_{\text{pr},0} \exp\left[-\frac{(t - n_{\text{pr}}z/c)^2}{\tau_{\text{pr}}^2}\right]$$

where  $n_{\text{pu}}, \alpha_{\text{pu}}, n_{\text{pr}}, \alpha_{\text{pr}}$  are pump and probe refractive indexes ( $n$ ) and absorption rates ( $\alpha$ ).

One finds

$$\begin{aligned} \Delta n(z, t) = & B\lambda_{\text{pr}} I_{\text{pu}, 0} \exp(-\alpha_{\text{pu}} z) \sum_{K=S, F} (C_K/\tau_{R, K}) \exp(\tau_{\text{pu}}^2/4\tau_{R, K}^2) \\ & \times \exp\left[-\frac{(t - n_{\text{pu}}z/c)}{\tau_{R, K}}\right] \\ & \times \left\{ 1 + \operatorname{erf}\left[\frac{(t - zn_{\text{pu}}/c - \tau_{\text{pu}}^2/2\tau_{R, K})}{\tau_{\text{pu}}}\right] \right\} \end{aligned} \quad (47)$$

and the phase variation  $\Delta\varphi$  reads

$$\begin{aligned} \Delta\varphi(l, t) = & \frac{2\pi}{\lambda_{\text{pr}}} \int_0^l \Delta n(z, t + n_{\text{pr}}z/c) dz \\ = & 2\pi B \int_0^l \exp(-\alpha_{\text{pu}} z) \sum_{K=S, F} (C_K/\tau_{R, K}) \\ & \times \exp\left(\frac{\tau_{\text{pu}}^2}{4\tau_{R, K}^2}\right) \exp\left[-\frac{(t + \beta z)}{\tau_{R, K}}\right] \\ & \times \left\{ 1 + \operatorname{erf}\left[\frac{(t + \beta z - \tau_{\text{pu}}^2/2\tau_{R, K})}{\tau_{\text{pu}}}\right] \right\} \end{aligned} \quad (48)$$

where  $\beta = (n_{\text{pr}} - n_{\text{pu}})/c$ . Thus, we can obtain the OKE signal ( $S$ ), with a delay  $\Delta t_{\text{pr}}$  between pump and probe pulses, by calculating the convolution product

$$S(\Delta t) = \exp(-\alpha_{\text{pr}} l) \int_{-\infty}^{+\infty} I_{\text{pr}}(\Delta t_{\text{pr}} - t') \sin^2 \frac{\Delta\varphi(t')}{2} dt' \quad (49)$$

*b. Results.* We report here the results concerning MBBA and MMA, MPA, and MBA, which have no nematic stable phases in the temperature range studied. The calculation of  $S(\Delta t)$  assumes the knowledge of both refractive indexes (at  $\lambda_{\text{pr}}$  and  $\lambda_{\text{pu}}$ ) and absorption rates at the same wavelengths. We measured the transmission of the studied compounds, at each temperature, for the pump and probe wavelengths. We found  $\alpha_{\text{pr}} \ll \alpha_{\text{pu}}$ , except in the vicinity of the phase transition, where the absorption is

mainly due to scattering. The obtained value of  $\alpha_{pu}$ , at 47°C and for MBBA, is  $16.4 \pm 0.8 \text{ m}^{-1}$ .

The refractive index of MBBA at  $\lambda_{pr}$  is deduced from earlier results [82];  $n(\lambda_{pu})$  is calculated by applying classical dispersion laws [15]. We found, always at 47°C,  $n_{pr} = 1.624 \pm 0.001$  and  $n_{pu} = 1.425 \pm 0.004$ . Thus, we calculated  $S(\Delta t)$  for different values of  $\tau_{R,F}$ , keeping  $\tau_{R,S}$  fixed at the value 100 ns, deduced from an earlier experiment at  $47.00 \pm 0.01^\circ\text{C}$  performed in our laboratory. We then measured the FWHH time and its variations with  $\tau_{R,F}$ . Results are reported in Fig. 16. This curve can be used to directly determine an approximate value of the relaxation time of the fast component from recorded OKE signals. Results are shown in Fig. 17. MBBA exhibits fast relaxations with  $\tau_{RF}$  lying in the 5-ps range, against a flat background which is obviously connected with the slow response ( $\tau_{R,S} = 100 \text{ ns}$ ). The ratio  $C_F/C_S$  has been found equal to  $(1.7 \pm 0.3) \times 10^{-3}$  at 47°C. Of course, it is impossible to go beyond this purely qualitative conclusion. MBPB (Fig. 18) exhibits a similar behavior, with perhaps a more marked tendency to many relaxations in the picosecond range. The three other compounds, which have no nematic phases, show only the fast relaxations with comparable HWHH times. These reorientation times are in agreement with the results of Rayleigh scattering investigations of Amer et al. [13] who reported bandwidths measured in the wings of the spectrum in the 3.5- to 5.5- $\text{cm}^{-1}$  range. (A reorientational time of 5 ps corresponds to a bandwidth of about 1  $\text{cm}^{-1}$ ). The variations in the intensity of the fast OKE signal and its FWHH time with

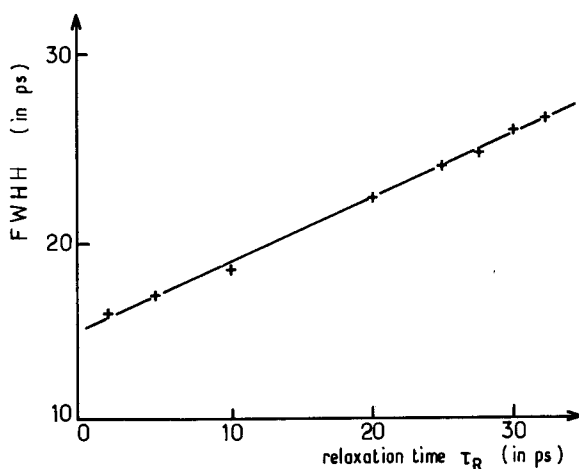
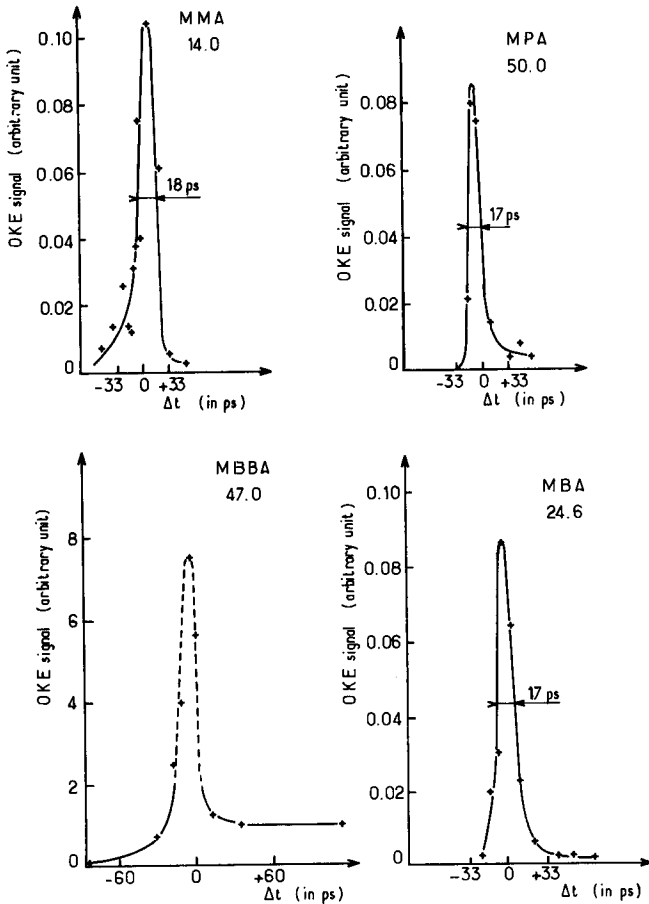


Figure 16. FWHH vs.  $\ln \tau_R$ . (After Ref. 15.)



**Figure 17.** OKE signals versus pump-probe delay  $\Delta t$ . MMA:  $94.00 \pm 0.01^\circ\text{C}$ ; MPA:  $50.00 \pm 0.01^\circ\text{C}$ ; MBA:  $24.60 \pm 0.01^\circ\text{C}$ ; MBBA:  $47.00 \pm 0.01^\circ\text{C}$ ;  $\tau_{\text{pu}} = 7 \pm 1$  ps;  $\tau_{\text{pr}} = 5 \pm 1$  ps; length of the cell: 4 cm. (After Ref. 15.)

temperature are reported in Fig. 19. As expected, both appear to be quite temperature independent.

OKE measurements performed in the isotropic phases of nematogens confirm the adequacy of both the de Gennes theory and the mean-field approximation to describe the response of such phases when submitted to intense optical fields. But, from both picosecond OKE and depolarized Rayleigh scattering investigations, it appears that fast contributions with no critical temperature dependence must be taken into account. These

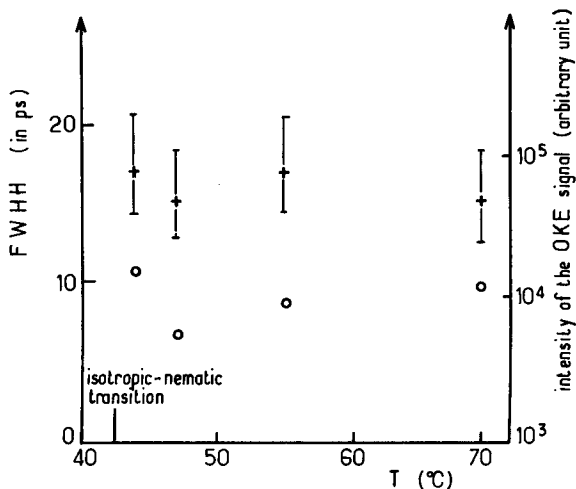


**Figure 18.** Variations of the intensity (o, right scale) and of the FWHM (+, left scale) of MBBA vs. temperature;  $\tau_{pu} = 7 \pm 1$  ps;  $\tau_{pr} = 5 \pm 1$  ps; length of the cell: 4 cm.

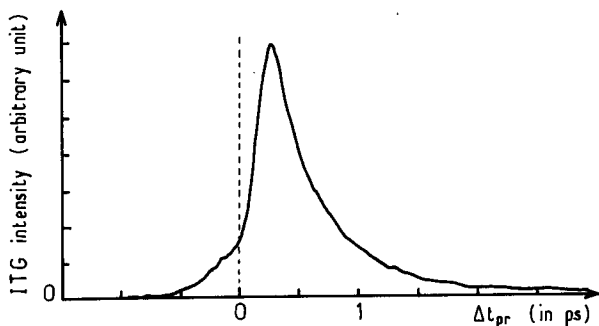


**Figure 19.** ITG signal (pure nuclear origin) versus probe delay. Compound: 5CB (*I* phase);  $t = (42.0 \pm 0.2)^\circ\text{C}$ ;  $\lambda_{pu} = \lambda_{pr} = 665$  nm;  $\tau_{pu} = \tau_{pr} \approx 200$  fs; thickness of the cell: 1 mm. (Reprinted from F. W. Deeg and M. D. Fayer, *J. Chem. Phys.* **91**, 2269 (1989), Fig. 8d, p. 2277.)

fast reorientations can probably be interpreted by involving local order fluctuations in the orientations of the correlated molecules in the phase. Of course, this work can only lead to an approximate value of the decay time (about 5 ps) of the “mean” fast relaxation. The two nematogens exhibit identical behavior, virtually temperature independent. We shall now see how these results have been recently confirmed and their accuracy enhanced by using subpicosecond ITG investigations.

## B. ITG Investigations

ITA investigations concern all the  $I$ ,  $N$ , and  $Sm-A$  phases. The last two phases have been studied in homeotropic alignment. The previous description of the OKE results of the  $I$  phases suggested the presence of many relaxations from the picosecond up to the microsecond range. We will see that such a complexity is also one of the main characteristics of these two much-ordered phases.

### 1. Isotropic Phases

We report here investigations of  $p$ - $n$ -pentyl- $p'$ -cyanobiphenyl (5CB) and  $p$ -cyanobenzylidene- $p$ -octyloxyaniline (CBOA) by Eyring and Fayer (EF) [83] and by Deeg, Fayer, et al. (DF) [84, 85]. EF used pump ( $\lambda_{\text{pu}} = 1064$  nm) and probe ( $\lambda_{\text{pr}} = 530$  nm) pulses of the duration  $\tau_{\text{pu}} = \tau_{\text{pr}} = 100$  ps. The pulse frequency was 400 Hz. The energy of the pumps was about 15  $\mu\text{J}$  (meanpower on the 280- $\mu\text{m}$ -thick sample: 14 mW). In the crossed polarization geometry, they observed results in very good agreement with those of the OKE. Slow relaxation ( $\tau_{\text{R,S}} = 60$  ns in 5CB at 42°C) was observed and a fast component, nonexponential and composed of a range of decay times from 2 ns down to the duration of the pulses, was evidenced. This fast relaxation is associated with individual rotational reorientation in “pockets” of different characteristics.

Five years later, DF developed a powerful and elegant technique using 50- $\mu\text{J}$ , 200 to 300-fs pulses, and a 1-kHz repetition rate at wavelengths of 575 and 665 nm, focused down to 120- $\mu\text{m}$  spot sizes (50  $\text{GW}/\text{cm}^2$ ). By varying both the angles between the pumps and detected signal polarizations, they were able to separate many contributions and, especially, to isolate pure nuclear reorientation. Figure 19 shows such a relaxation obtained with 5CB sample, 1 mm thick. While reorientational relaxation seems not to be hydrodynamical (it cannot be described in terms of the Debye model and displays complex dynamics up to 200 ps), the “mean” relaxation time appears to be about 1 ps. This is exactly what can be predicted from rotational hydrodynamics of species with a moment of inertia of about  $10^{-13}$  g/cm, associated to viscosity of about  $10^{-1}$  P, a typical value in  $I$  phases. A model describing such complex relaxations has been proposed. Values less than 1 ps are probably associated with intramolecular rotations of atom groups in the molecule. Moreover, the observed behavior is weakly temperature dependent down to the  $I \rightleftharpoons N$  phase transition. This beautiful experiment brings quantitative confirmation of the pioneering OKE work, performed fifteen years ago with less highly evolved techniques.



## 2. Nematic Phases

Under laser pulses from cw to a nanosecond regime, the third-order nonlinearities are mainly due to director-axis reorientation and thermal or densities changes. These slow responses, which may be very useful in optical applications of liquid crystals, have been intensely studied lately [5, 87–90]. They also appear in picosecond-induced gratings as recently demonstrated by Eichler and Macdonald (EM) [91], and Khoo et al. [90]. EM used 80-ps pulses, at  $\lambda_{pu} = 532$  nm, with crossed polarizations and a cw probing wave at  $\lambda_{pr} = 488$  nm. The energy of the pumps was less than 1 mJ. Slow effects with rise and decay times respectively some tens of nanoseconds and milliseconds were observed. The rise time is explained by the pump-induced director deformation of the phase, associated with laser induced flow, while the relaxation is governed by the visco-elastic properties of the sample. These slow effects generally occur when the pump electric field exhibits a component in the direction of the director  $\mathbf{n}$  of the phase. In the EM experiment  $(\mathbf{k}_{pu}, \mathbf{n}) = 22.5^\circ$  and the nematic barrier [92] was overcome. Khoo used 66-ps pulses at  $\lambda_{pr} = 532$  nm.

If the wave vectors of the pumps are almost parallel to the director, these slow responses strongly decrease in the case of orthogonal polarizations of the pumps [91]. EF observed that the slow component of the Kerr relaxation disappears. This was interpreted in terms of onset of the

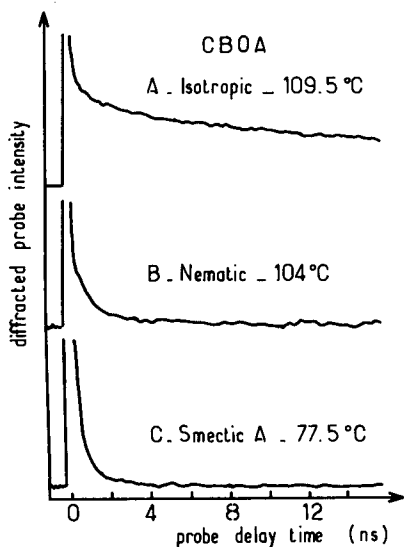


**Figure 20.** ITG signal versus probe delay. Compound: CBOA;  $\lambda_{pu} = 1064$  nm;  $\lambda_{pr} = 532$  nm;  $\tau_{pu} = \tau_{pr} \approx 100$  ps; thickness of the cell:  $280 \mu\text{m}$ . (Reprinted from G. Eyring and M. D. Fayer, *J. Chem. Phys.* **81**, 4314 (1984) Fig. 4, p. 4318.)

namatic barrier, the optical torques not being sufficient to produce the collective slow rotation of the molecules. But the fast relaxations remain measurable, despite a strong reduction of their amplitude (by a factor of 10), as shown in Fig. 20. We see in the next section that we have confirmed this reduction from the  $I$  to the  $N$  phase with our DFWM experiments.

### 3. *Smectic-A Phases*

As far as we know, the only work remaining is that of EF (Fig. 20). As in the  $N$  phase, the slow component does not appear. The fast relaxations are slightly reduced in amplitude (by a factor of 3) and the FWHH time approaches the same order of magnitude as the response time of the detection, showing a more pronounced evolution toward pure individual molecular relaxations.

### C. DFWM Investigations [95, 96]

Before describing our experimental setup, let us mention here the pioneering work of Yariv et al. [93], who used the large and nonresonant third-order susceptibility of the  $I$  phases to perform DFWM investigation, and that of Madden et al. [94], who used 25-ns pulses at 1064 nm to study  $I$  samples of 1 cm thickness by using the same technique. Our experimental setup is described in Fig. 21. We used a simultaneously  $Q$ -switched and mode-locked home-made YAG laser. The mode-locking mode was performed by using an acousto-optic mode locker coupled to passive dye locking. A single pulse ( $\lambda = 1060$  nm:  $\tau = 25$  ps) was selected from the first half of the pulse train by a Pockels single-pulse selector at a 1-Hz frequency rate. After amplification by a double passing YAG amplifier, a second-harmonic generator produced single green ( $\lambda = 530$  nm) pulses of about 1 mJ energy. An expanding telescope was used to increase the diameter of the selected  $TEM_{00}$  mode up to about 3.5 mm. These pulses were monitored by a fast photodiode coupled to a fast digitizer that triggered the signal acquisition of a computer that drove the laser, the mechanical drivers, the photon counting devices, and performed the mathematical treatment of the results. The two pump and probe waves were separated by several beamsplitters and sent on the 250- or 500- $\mu$ m samples after a reduction of their diameter to about 1.5 mm. The intensities of the two pumps and the probe were respectively about 200 and 100  $\mu$ J when they reached the sample (500 MW/cm<sup>2</sup>). The sample was placed inside an oven where the temperature was regulated to  $\pm 0.01$  K. The probe and the first pump can be delayed by mechanical drivers. The distance length between the sample and the photon-counting device was about 3 m. This distance, together with the pinhole (diameter about 5 mm) placed in front of the detector, largely reduced the spurious signals coming

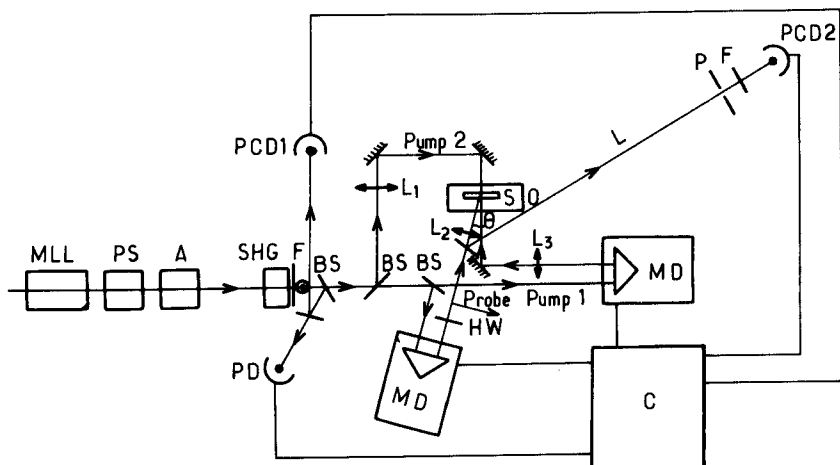


**Figure 21.** DFWM experimental setup. MLL, mode-locked laser; PS, pulse selector; A, double-scan amplifier; SHG, second-harmonic generator; F, interference filters;  $\lambda = 530$  nm; BS, beamsplitters; HW, half-wave plate,  $\lambda = 530$  nm; S, sample; O, oven; PD, fast photodiode; PCD, photon counting device; C, computer; MD, mechanical delays; P, pinhole,  $\phi \approx 5$  mm;  $L \approx 3$  m;  $\theta \approx 7^\circ$ ;  $L_1$ , lens  $f = 50$  cm;  $L_2$ , lens  $f = 16$  cm;  $L_3$ , lens  $f = 40$  cm. (After Ref. 96.)

from all the components of the setup, thus affording the detection of the DFWM signal on a very weak background. At each laser pulse, the laser wave intensity was monitored, allowing the necessary check of the signal dependence with the third power of the laser intensity. Because of this power law, the laser intensity stability must be carefully controlled. An accurate adjustment of the oscillator cavity length, as required by the active mode-locking, yielded a ratio of about 0.05 of the standard deviation and the signal. Spurious laser pulses, which can sometimes occur, were rejected by the computer. The linear transmission of the material was carefully controlled for the laser pump before investigation.

The third-order polarization  $P^{(3)}(t)$  can be written (in the hypothesis of two relaxations)

$$P^{(3)}(t) = E_{\text{pu},2}(t) \int_{-\infty}^t f_2(t-t') E_{\text{pr}}(t' - \Delta t_{\text{pr}}) E_{\text{pu},1}(t' - \Delta t_{\text{pu}}) dt' \quad (50)$$

where  $\Delta t_{\text{pr}}$  and  $\Delta t_{\text{pu},1}$  are the delays of the probe and pump 1 with respect to pump 2, chosen as the time reference. The intensity of the

backward wave is given by

$$I_{\text{BW}} \propto \int_{-\infty}^{+\infty} |P^{(3)}(t)|^2 dt \quad (51)$$

The polarization of the probe and the pump are crossed. Thus, it appears that  $I_{\text{BW}}$  is basically a function of the relaxation constant ( $s$ )  $\tau_R$  involved in  $f_2(t)$ ,  $\Delta t_{\text{pu}}$ , and  $\Delta t_{\text{pr}}$ . It will be denoted by  $I_{\text{BW}}(\tau_R, \Delta t_{\text{pu}}, \Delta t_{\text{pr}})$ .

The natural method for measuring  $\tau_R$  (method 1) is to plot  $I_{\text{BW}}(\tau_R, \Delta t_{\text{pu}}, 0)$  versus  $\Delta t_{\text{pu}}$ . Figure 22 reports a computer simulation of the variations of  $I_{\text{BW}}(\tau_R, \Delta t_{\text{pu}}, 0)$  versus  $\Delta t_{\text{pu}}$ , in the simplified case where self-modulation is absent ( $a = 0$  in Eq. (27)). The duration  $\tau$  of the pulses was held fixed at 25 ps. As expected, the signal duration increases with  $\tau_R$ . But it is possible to determine accurately  $\tau_R$  from the measurement of FWHH only if  $\tau_R \gg \tau$ . Unfortunately, in this work  $\tau \approx \tau_R$  and the measurements of  $\tau_R$  with this method cannot be accurately performed. However, it will be used later.

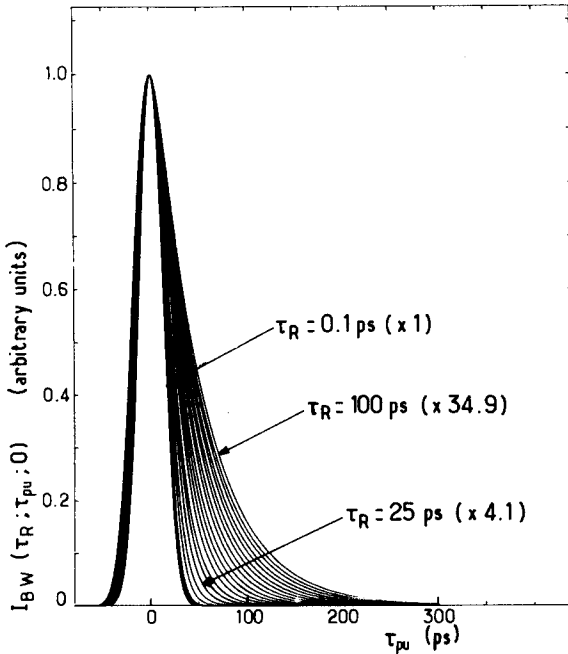
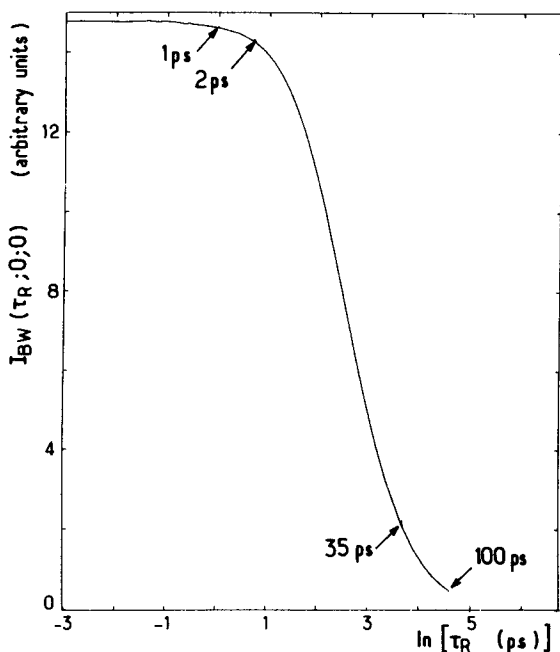


Figure 22.  $I_{\text{BW}}(\tau_R; \Delta t_{\text{pu}}, 0)$  vs.  $\Delta t_{\text{pu}}$  for same values of  $\tau_R$ ; the amplitude is normalized to 1. (After Ref. 96.)



**Figure 23.**  $I_{BW}(\tau_R; 0; 0)$  vs.  $\tau_R$ ;  $\tau = 25$  ps;  $a = 0$ . The amplitude of the response function  $f_2$  is assumed to be constant. (After ref. 96.)

For  $\Delta t_{pr} = \Delta t_{pu,1} = 0$ , the three pulses reach the sample at the same time. Thus, Eq. (51) becomes

$$P^{(3)}(t) = E_{pu,2}(t) \int_{-\infty}^{+t} f_2(t-t') E_{pr}^*(t') E_{pu,1}(t') dt' \quad (52)$$

In this case

$$E_{pr}^*(t') E_{pu,1}(t') = |\varepsilon(t')|^2 = \exp[-4 \ln 2 (t'/\tau)^2] \quad (53)$$

and  $I_{BW}(t) \approx |P^{(3)}(t)|^2$  becomes phase-modulation independent.

A computer simulation (Fig. 23) shows that, in this case, the amplitude  $I_{BW}(\tau, 0, 0)$  strongly decreases when  $\tau_R$  increases in the pertinent time domain (1–100 ps). Then, the second method, i.e., plotting the variations of  $I_{BW}(\tau_R, 0, \Delta t_{pr})$  versus  $\Delta t_{pr}$  and taking the maximum value  $I_{BW}(\tau_R, 0, 0)$ , can be used for evaluating  $\tau_R$  by computer simulation. This

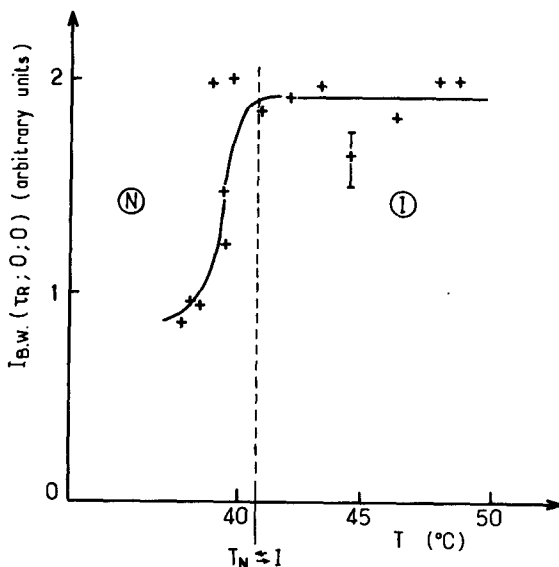


**Figure 24.**  $I_{BW}(\tau_R; 0; 0)$  vs. temperature. Compound: 8CB; thickness of the sample: 200  $\mu\text{m}$ ;  $\lambda_{pu} = \lambda_{pr} = 532$  nm;  $\lambda_{pu} = \lambda_{pr} \approx 25$  ps.

second method obviously will reveal only fast reorientations in the range of some tens of picoseconds.

Let us now report our main results.

### 1. Isotropic and Nematic Phases

For 8CB in the  $I$  phase,  $I_{BW}(\tau_R, 0, 0)$  appears to be temperature independent down to the  $I \rightleftharpoons N$  phase transition, where the signal suddenly decreases by a factor of about 2.5. The decrease occurs because of (1) the reduction of the effective anisotropy  $\gamma_{\text{eff}}^2$ , connected with the increased hindrance of the rotations about the short molecular axes in the homeotropic  $N$  phase (in  $I$  phases, the highest first-order polarizability along the long molecular axis plays an important role that is forbidden in the  $N$  phase) and (2) the sudden increase of the shear viscosity at the  $I \rightarrow N$  transition [97]. Figure 24 illustrates this important reduction. No such change appears at the  $N \rightleftharpoons Sm-A$  phase transition.

### 2. Smectic A Homeotropic Phases

In the picosecond range, the DFWM signal is mainly induced by the reorientations about the long molecular axis, which, as already mentioned in the introduction, are associated to biaxiality, and to ferroelectricity in

*Sm-C\** phases (which are basically biaxial phases, as shown in Fig. 6). They are associated with the second-rank tensor  $\Delta\epsilon$  describing the fluctuations of the dielectric constant and, more especially, to  $\Delta\epsilon_{yx}$  for the homeotropic *Sm-A* phase oriented according to Fig. 6. These fluctuations can be called in-plane fluctuations, by reference to the layer planes. They appear to be basically connected to the already introduced restricted effective optical anisotropy  $\gamma_{\perp,\text{eff}}^2 = (\alpha_{\perp,1,\text{eff}} - \alpha_{\perp,2,\text{eff}})^2$ . Then, keeping the orientational situation described in Fig. 6, the corresponding response of *Sm-A* phases to picosecond pulses, driving optical fields linearly polarized in the *XY* plane, is of the fast type and can be written

$$f_3(t) \propto \rho \mathcal{L} \frac{\gamma_{\perp,\text{eff}}^2}{kT \tau_{R,F}} \exp\left(t - \frac{t}{\tau_{R,F}}\right) = \frac{C'_F}{\tau_{R,F}} \exp\left(\frac{-t}{\tau_{R,F}}\right) \quad (54)$$

All the parameters of this equation have already been defined. In fact, the situation appears to be more complicated. We have recently shown [98], both theoretically and experimentally, that because of the fluctuations of both **N** and **n** with respect to the laboratory axis *Oz* (see Fig. 6), there appears an additional contribution to  $\Delta\epsilon_{yx}$  leading to an additional term  $\chi_{\text{ani,S}}^{(3)}$  which can be written, far from the *Sm-A*  $\rightleftharpoons$  *N* phase transition,

$$\chi_{\text{ani,S}}^{(3)} \propto \Delta\epsilon_a(kT) \left[ \frac{A_1}{\sqrt{\tilde{B}\delta k_i^3}} + \frac{A_2}{\sqrt{Dk_i^3}} \right]^{1/2} \quad (55)$$

where  $\Delta\epsilon_a$  denotes the anisotropy ( $\epsilon_{\parallel} - \epsilon_{\perp}$ ) of the dielectric constant at optical frequencies,  $A_1$  and  $A_2 \approx A_1/10$  are constants;  $\tilde{B}$  and  $D$  respectively describe layer compressibility and reorientation of the director [1];  $k_i$  and  $\delta k_i$  are generic notations for the Franck constants of the phase [99]. These contributions diverge at the *Sm-A*  $\rightleftharpoons$  *N* phase transition. The associated relaxation times are of the slow type, but have not been measured at this time. The whole response function is then of the type

$$f_4(t) = \frac{C'_F}{\tau_{R,F}} \exp\left(\frac{-t}{\tau_{R,F}}\right) + \frac{C'_S}{\tau_{R,F}} \exp\left(\frac{-t}{\tau_{R,S}}\right) \quad (56)$$

which looks like Eq. (44), but with the difference that  $C'_F \propto \gamma_{\perp,\text{eff}}^2$ , while  $C_F \propto \gamma_{\text{eff}}^2$ . Moreover, the temperature dependences of  $C_S$  and  $C'_S$  differ strongly.

The DFWM signal appears to be very small. We have chosen  $CS_2$  as a reference, because of its importance as a nonlinear standard. We have

obtained a mean ratio for the signals given by CS<sub>2</sub> and 8CB about 18 ± 2. 8CB was studied at 31.5°C, i.e., in the *Sm-A* phase. One must evaluate the ratio  $(C_{F,CS_2}/C'_{8CB})^2$  by using the second method already cited. In this case,

$$I_{BW}(\tau_{R,F}, 0, \Delta t_{pr}) = \frac{C_F'^2}{\tau_{R,F}^2} \int_{-\infty}^{+\infty} \varepsilon^2(t) \times \left[ \int_{-\infty}^{+\infty} \exp - [(t - t')/\tau_{R,F}] \varepsilon(t' - \Delta t_{pr}) \varepsilon(t') dt' \right]^2 dt \quad (57)$$

With the numerical values  $\rho_{CS_2} = 10^{22} \text{ cm}^{-3}$  [100],  $\rho_{8CB} = 2.0 \times 10^{21} \text{ cm}^{-3}$  [101],  $n_{CS_2} = 1.673$  [100],  $n_{8CB} = 1.56$  [102],  $\gamma_{CS_2}^2 = 117 \times 10^{-48} \text{ cm}^6$  [35],  $\gamma_{\perp,8CB}^2 = 441 \times 10^{-48} \text{ cm}^6$  [103], and taking  $\mathcal{L} = (n^2 + \frac{2}{3})^4$  [94], we find a ratio of about 2.8, i.e., 6.4 times smaller than the one measured. Therefore, the slowing down factor, due to a larger  $\tau_{RF}$  for 8CB as compared to CS<sub>2</sub>, is about 6.4. If one refers to Fig. 23 and to the 2-ps reorientational time of CS<sub>2</sub>, one finds for 8CB at 31.5°C in the *Sm-A* phase,  $\tau_{R,F} \approx 35$  ps. We checked this value using the first method; the results are given in Fig. 25. As expected, in the 28–34°C temperature range, we find a quite linear variation of  $\ln I_{BW}(\tau_{R,F}, \Delta t_{pu}, 0)$  versus  $\Delta t_{pu}$  leading to a FWHH of about 30 ps. Of course, this linear behavior, observed over only one decade, does not prevent slower relaxations from occurring for larger values of  $\Delta t_{pu}$ . But, in this case, the signal-to-noise ratio strongly decreases and we cannot perform accurate determinations of the slower rates. The fastest one recorded can be interpreted as the time describing rotational librations of individual molecules about their long axis, modified by short-range coupling to neighboring particles. In the frequently used models of rotational relaxation in dense media composed of rodlike molecules [56, 104, 105], these fast components are associated with reorientation of the rod within the cylinder formed by its nearest neighbors. These models also include slower components generated by the rotational diffusion of the cylinder (coupled rotations of some tens of particles) with associated times in the range of some hundreds of picoseconds. These times have been obtained by FIR [19] as well as by time domain spectroscopy and significantly slow down upon entering the *Sm-C* phase (from 342 ps in *Sm-A* to 517 ps in *Sm-C* [20]).

We have not detected any decrease of  $I_{BW}$  down to the *Sm-A*  $\rightleftharpoons$  *Sm-C* phase transition [95, 96] for compound 6, which is achiral. However, for compound 5, a ferroelectric chiral mixture, we observe an important decrease of  $I_{BW}(\tau_{R,F}, 0, 0)$  in the last degree before the transition. Figure 26 reports the results for compounds 5 and 6. Our observations suggest the



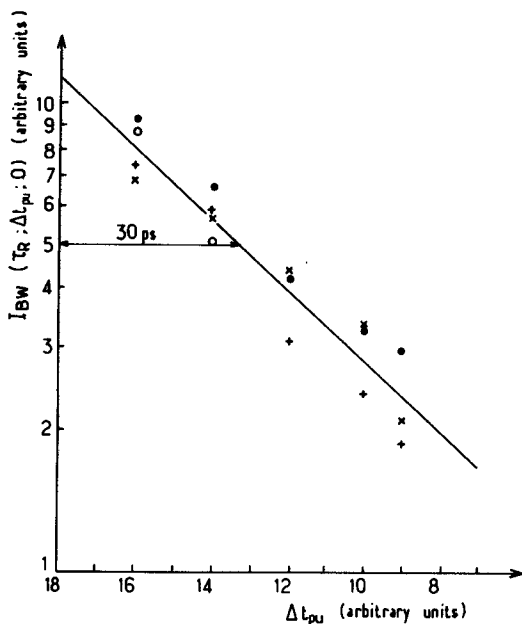


**Figure 25.**  $I_{BW}(\tau_R; \Delta t_{pu}; 0)$  vs.  $\Delta t_{pu}$ . Compound: 8CB in the  $Sm-A$  phase; thickness of the sample:  $200 \mu\text{m}$ ;  $\lambda_{pu} = \lambda_{pr} = 532 \text{ nm}$ ;  $\tau_{pu} = \tau_{pr} \approx 25 \text{ ps}$ . (After Ref. 96.)

presence of a pretransitional  $Sm-C^*$  effect in the  $Sm-A^*$  phase, in the vicinity of the phase transition, an idea supported by recent studies of ferroelectric liquid crystals dynamics, showing helical fluctuations far under the  $Sm-C^* \rightleftharpoons Sm-A^*$  transition, and by X-ray investigations showing  $Sm-C^*$  density modulations inside a 1-K temperature range across the transition [106]. In spite of the fact that we have not proved that  $C'_F$  does not decrease in the vicinity of the  $Sm-C^*$  phase, the observed effect appears to be more probably connected to a two- or threefold increase of  $\tau_{R,F}$  in the last degree of the  $Sm-A^*$  phase, in agreement with the idea of a slowing down of the rotation about the long molecular axis in ferroelectric phases [107]. This means that the isotropic rotation in the  $Sm-A^*$  phase is largely modified near the ferroelectric phase, the short molecular axes spending more and more time in some privileged directions. In this case,  $\tau_{R,F}$ , which gives only an effective macroscopic view of the rotational relaxation, increases.

The theory of the effect [96] leads to an increase of the effective time given by

$$\tau_{R,F,\text{eff}} = [1/\tau_{R,F} - B/(T - T_c)]^{-1} \quad (58)$$

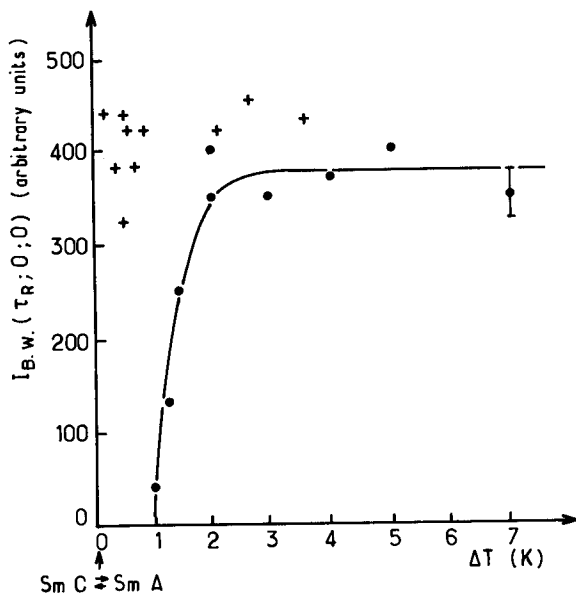


**Figure 26.**  $I_{BW}(\tau_R; 0; 0)$  vs. temperature. Thickness of the sample:  $500 \mu\text{m}$ ;  $\lambda_{pu} = \lambda_{pr} = 532 \text{ nm}$ ;  $\tau_{pu} = \tau_{pr} \approx 25 \text{ ps}$ ; +, compound 6 of Table 3; ●, compound 5 of Table 3.

where  $B$  is a constant and the fit of our experimental results by Eq. (58) leads to  $\tau_{R,F} \approx 20 \text{ ps}$ ;  $B \approx 4.4 \times 10^{-2} \text{ ps}^{-1} \text{ K}$ .

We must note here that an alternative interpretation of our work has been proposed [108] and a recent OKE investigation of the same mixture has not confirmed our observation [109]. However, it must be pointed out that this OKE investigation was performed with an inducing wave of high power (many watts), strongly focused in the sample (beam-waist of  $80 \mu\text{m}$ ), at a wavelength ( $1.053 \mu\text{m}$ ) where liquid crystals absorb, and mode-locked at a very high repetition rate (100 MHz). These strong differences between the two experiments can perhaps explain the different results obtained. For instance, the OKE signal for 8CB, at zero delay between pump and probe, is reported to be three times larger than that from  $\text{CS}_2$ , while our DFWM signal from 8CB was 18 times smaller than the corresponding one from  $\text{CS}_2$ . A ratio larger than 1 cannot be explained from numerical evaluation of the contribution due to pure molecular reorientation about the long axis. As reported before, the calculated amplitude ratio is about 0.36, and the difference between reorientational times (8CB: some tens of ps;  $\text{CS}_2$ : 2 ps) still diminishes the value of the ratio.

Moreover two recent DS experiments performed on pure compounds, near 1 GHz, give opposite results. The first (110, 111) does not show any

variation of the relaxation frequency from 10 K above the  $Sm-A \rightleftharpoons I^*$  transition, all across the  $Sm-C^*$  phase down to the crystal, in contrast to previous results [112]. The second is interpreted as invoking a component that slows down near the ferroelectric phase [113]. But, none of the DS experiments seem to probe pure individual reorientation.

Finally, let us point out that Eq. (58) is deduced from a model involving a coupling ( $B$  constant) between laser-induced biaxiality and fluctuating permanent polarization in the cybotactic ferroelectric groups appearing in the  $Sm-A^*$  phase. Then, the role played by the molecular transversal permanent dipoles, which are responsible for the ferroelectricity, is determinant. Compound 7, which is a racemic mixture without permanent transversal polarization, does not give any coupling ( $B = 0$ ) and, as expected, the corresponding  $I_{BW}$  does not reveal any noticeable decrease down to the  $Sm-C$  phase [96].

Thus, we have presented results of DFWM on  $I$ ,  $N$ , and  $Sm-A$  phases consisting of chiral, achiral, or racemic species. In  $I$  phases, a time-unresolved temperature-independent response has been detected. It slows down at the  $I \rightleftharpoons N$  phase transition in agreement with the observations resulting from ITG investigations. Signals monitored in homeotropic  $N$  and  $Sm-A$  phases reveal complex relaxations, the main signal having probably been due to individual molecular reorientations about the long molecular axis, affected by local order. In chiral compound,  $I_{BW}$  falls near the ferroelectric phase, probably in connection with a shift of the mean relaxation time toward longer times. This effect is interpreted as being due to a coupling between the fluctuating permanent polarization and the transient biaxial mode, induced by the laser field in the cybotactic groups of molecules [96]. Achiral and racemic compounds do not present this pretransitional behavior, which seems directly connected to the vicinity of the ferroelectric  $Sm-C^*$  phase.

## VI. GENERAL CONCLUSIONS AND PROSPECTS

We have tried to show the interest of nonlinear optics in studies of the fast reorientations in liquid crystals. Actually, only the isotropic phase seems to be correctly investigated. In addition to the de Gennes contribution,  $I$  phases exhibit a distribution of orientational relaxation times, ranging from some hundreds of femtoseconds up to some hundreds of picoseconds with a mean relaxation time of a few picoseconds. The ITG technique [85, 86] has given the most accurate results, in agreement with older OKE investigations. Such results are in good agreement with the pioneering work, both theoretical [114] and experimental (Rayleigh scattering) of Shen et al. [13]. The exact origin of this new reorientational dynamics remains an open question. Reorientation times less than some picoseconds

can be due to intramolecular dynamics. Times of some tens or hundreds of picoseconds probably arise from orientational fluctuations of individual molecules modified by coupling with neighboring particles. The decay rates can strongly change—by orders of magnitude—according to the duration of the laser pulses used. Thus, subpicosecond pulses are needed, as in the Fayer work, with the additional conditions (1) that the electronic contribution can be accurately separated from the nuclear one, and (2) that the extremely high values of the optical fields delivered by these very short pulses do not lead to undesirable effects in the compounds and thus to erroneous interpretations.

The homeotropic  $N$  and  $Sm-A$  phases cannot be correctly oriented in samples of more than 500- $\mu\text{m}$  thickness (except in free-surface geometry, which has recently allowed us to obtain 2.5-mm  $Sm-A^*$  phases of good optical quality). Thus, OKE and ITG induced by subpicosecond pulses generally lead to poor signal-to-noise ratios. DFWM appears to be a more useful technique, because of its high efficiency. It has allowed us to study the orientational in-plane fluctuations in the  $Sm-A$  phases, thus opening the investigations of pretransitional behavior in relation with the ferroelectric order exhibited by  $Sm-C^*$  phases. But the separation of the different processes involved appears to be rather difficult in these anisotropic phases. Here, also, the use of subpicosecond pulses might be useful to solve the still open question concerning the molecular origin of ferroelectricity in liquid crystals. Finally, let us note that the nonlinear techniques already mentioned could be applied to the study of the recently discovered  $Sm-O^*$  [115] and  $Sm-C_{A^*}$  [116] phases, the exact nature of which are still unknown, and which appear to be optically equivalent to biaxial  $Sm-A$  phases.

### References

1. P. G. De Gennes, *The Physics of Liquid Crystals*, Clarendon, Oxford, UK, 1974.
2. R. M. Herman and R. J. Serinko, *Phys. Rev. A* **19**, 1757 (1979).
3. A. S. Zolot'ko, V. F. Kitaeva, N. Kroo, N. N. Sobolev, and L. Chillag, *Pis'ma Zh. Eksp. Teor. Fiz.* **32**, 170 (1980) (*JETP Lett.* **32**, 158 (1980)).
4. See, for example, S. M. Arakelian, and Y. S. Chilingarian, *Non Linear Optics of Liquid Crystals*, Nauka, Moscow, 1984; I. C. Khoo, *Prog. Opt.* **26**, 105 (1988); E. M. Averyanow and M. A. Osipov, *Usp. Fiz. Nauk* **160**, 89 (1990).
5. S. D. Durbin, S. M. Avakelian, and Y. R. Shen, *Phys. Rev. Lett.* **47**, 1411 (1981).
6. Mi-Mee Cheung, S. D. Durbin, and Y. R. Shen, *Opt. Lett.* **8**, 39 (1983).
7. H. Hsiung, L. P. Shi, and Y. R. Shen, *Phys. Rev. A* **30**, 1453 (1984).
8. I. C. Khoo and Y. R. Shen, *Opt. Eng.* **24**, 579 (1985).
9. H. J. Eichler and R. Macdonald, in R. C. Sze and F. J. Duarte (Eds.), *Proceedings of the International Conference on Lasers 88*, STS Press, McLean, VA, 1989.

10. See S. Chandrasekhar, *Liquid Crystals*, Cambridge UP, Cambridge, UK, 1977, Chapter 3.
11. H. J. Eichler and R. Macdonald, *Phys. Rev. Lett.* **67**, 2666 (1991).
12. J. R. Lalanne, *Phys. Lett.* **51A**, 74 (1975).
13. N. M. Amer, Y. S. Lin, and Y. R. Shen, *Solid State Commun.* **16**, 1157 (1975).
14. J. R. Lalanne, B. Martin, B. Pouligny, and S. Kielich, *Opt. Commun.* **19**, 440 (1976).
15. J. R. Lalanne, B. Martin, B. Pouligny, and S. Kielich, *Mol. Cryst. Liq. Cryst.* **42**, 153 (1977).
16. J. A. Janik, M. Godlewska, T. Grochulski, A. Kocot, E. Sciesinska, J. Sciesinski, and W. Witko, *Mol. Cryst. Liq. Cryst.* **98**, 67 (1983).
17. F. Volino, A. J. Dianoux, and A. Heideman, *J. Phys. Lett.* **40**, 583 (1979).
18. A. J. Leadbetter, J. M. Richardson, and J. C. Frost, *J. Phys. Colloq.* **40**, 125 (1979).
19. J. A. Janik, J. Krawczyk, J. M. Janik, and K. Otnes, *J. Phys. Colloq.* **40**, 169 (1979).
20. J. Chrusciel and W. Zajac, *Liq. Cryst.* **10**, 419 (1991).
21. A. Nayeem and J. H. Freed, *J. Phys. Chem.* **93**, 6539 (1989).
22. J. W. Emslev and C. A. Veracini, *NMR in Liquid Crystals*, Reidel, Dordrecht, 1985.
23. See, for example, B. J. Berne and R. Pecora, *Dynamic Light Scattering*, Wiley, New York, 1976; M. W. Evans, *Simulation and Symmetry in Molecular Diffusion and Spectroscopy*, *Adv. Chem. Phys.* **81**, 361 (1992) (I. Prigogine and S. A. Rice, (Eds.), Wiley, New York).
24. A. D. Buckingham, *Proc. Phys. Soc.* **B69**, 344 (1956).
25. G. Mayer and F. Gires, *C. R. Acad. Sci. Paris* **258**, 2039 (1961).
26. S. Kielich, *Acta Phys. Pol.* **30**, 683 (1966); **31**, 689 (1967).
27. H. J. Eichler, Special Issue on Dynamic Gratings and Four Waves Mixing, *IEEE J. Quantum Electron.* **QE-22**, 1194 (1986).
28. R. W. Hellwarth, *J. Opt. Soc. Am.* **67**, 1 (1977).
29. B. Kasprowicz-Kielich, S. Kielich, and J. R. Lalanne, in J. Lascombe (Ed.), *Molecular Motions in Liquids*, Reidel, Dordrecht, 1974, p. 563.
30. W. Voigt, *Magneto-und Electro-Optik*, Teubner, Leipzig, 1908.
31. M. Born, *Optik*, Springer, Berlin, 1933.
32. P. Debye, *Polare Molekeln*, Leipzig, 1929.
33. W. Alexiewicz, J. Buchert, and S. Kielich, *Acta Phys. Pol.* **A52**, 445 (1977).
34. B. F. Levine and C. G. Bethea, *J. Chem. Phys.* **63**, 2666 (1975).
35. See, for example, J. R. Lalanne, *J. Phys.* **30**, 643 (1969); S. Kielich, *Proc. Indian Acad. Sci. (Chem. Sci.)* **94**, 403 (1985).
36. J. R. Lalanne, B. Lemaire, J. Rouch, C. Vaucamps, and A. Proutiere, *J. Chem. Phys.* **73**, 1927 (1980).
37. P. Papffy-Muhoray, H. J. Yuan, L. Li, M. A. Lee, J. R. Desalvo, T. H. Wei, M. Sheik-Bahae, D. J. Hagan, and E. W. Van Stryland, *Mol. Cryst. Liq. Cryst.* **207**, 291 (1991).
38. M. J. Soileau, T. H. Wei, M. Sheik-Bahae, D. J. Hagan, M. Sence, and E. W. Van Stryland, *Mol. Cryst. Liq. Cryst.* **207**, 97 (1991).
39. M. J. Soileau, E. W. Van Stryland, S. Guha, E. J. Sharp, G. L. Wood, and J. L. W. Pohlmann, *Mol. Cryst. Liq. Cryst.* **143**, 139 (1987).

40. M. J. Soileau, S. Guha, W. E. Williams, E. W. Van Stryland, and H. Vanherzeele, *Mol. Cryst. Liq. Cryst.* **127**, 321 (1985).
41. R. Risser, D. W. Allender, M. A. Lee, and K. E. Schmidt, *Mol. Cryst. Liq. Cryst.* **179**, 335 (1990).
42. J. P. Hermann, D. Ricard, and J. Ducuing, *Appl. Phys. Lett.* **23**, 178 (1973).
43. J. R. Lalanne and P. Bothorel, *J. Chim. Phys.* **11**, 1538 (1966).
44. G. R. Alms, T. D. Gierke, and W. H. Flygare, *J. Chem. Phys.* **61**, 4083 (1974).
45. A. K. Burnham, G. R. Alms, and W. H. Flygare, *J. Chem. Phys.* **62**, 3289 (1975).
46. D. Kivelson and P. A. Madden, *Annu. Rev. Phys. Chem.* **31**, 523 (1980).
47. T. Keyes and B. M. Ladanyi, *Mol. Phys.* **34**, 765 (1977).
48. S. J. Bertucci, A. K. Burnham, G. R. Alms, and W. H. Flygare, *J. Chem. Phys.* **66**, 605 (1977), T. D. Gierke, *J. Chem. Phys.* **65**, 3873 (1976).
49. M. E. Rose, *Elementary Theory of Angular Momentum*, Wiley, New York, 1967.
50. L. Van Hove, *Phys. Rev.* **95**, 249 (1954).
51. See, for example, B. Kasprowicz and S. Kielich, *Acta Phys. Pol.* **33**, 495 (1968); S. Kielich, *J. Colloid Interface Sci.* **33**, 142 (1970); S. Kielich, J. R. Lalanne, and F. B. Martin, *J. Phys.* **33**, C1-191 (1972); M. W. Evans, S. Wozniak, and G. Wagniere, *Physica B* **175**, 412 (1991). In Eq. 13, the negative, zero, and positive values of  $J_A$  successively describe the diatropic, atropic, and paratropic behaviors, according to the terminology introduced by J. A. Prins and W. Prins, *Physica* **23**, 253 (1957).
52. F. B. Martin and J. R. Lalanne, *Opt. Commun.* **2**, 219 (1970).
53. F. B. Martin and J. R. Lalanne, *Phys. Rev. A* **4**, 1275 (1971).
54. J. R. Lalanne, F. B. Martin, and P. Bothorel, *J. Colloid Interface Sci.* **39**, 601 (1972).
55. D. R. Bauer, G. R. Alms, J. I. Brauman, and R. Pecora, *J. Chem. Phys.* **61**, 2255 (1974).
56. P. D. Maker, *Phys. Rev. A* **1**, 923 (1970).
57. R. H. Cole, *J. Chem. Phys.* **42**, 637 (1965).
58. K. B. Eisenthal and K. H. Drexhage, *J. Chem. Phys.* **51**, 5720 (1969).
59. T. J. Chuang and K. B. Eisenthal, *Chem. Phys. Lett.* **11**, 368 (1971).
60. C. V. Shank and D. H. Auston, *Phys. Rev. Lett.* **34**, 479 (1975).
61. J. R. Lalanne and R. Lefebvre, *J. Chim. Phys.* **73**, 337 (1976).
62. J. Etchepare, G. Grillon, J. P. Chambaret, G. Harmoniaux, and A. Orszag, *Opt. Commun.* **63**, 329 (1987).
63. A. Yariv, *Opt. Commun.* **25**, 23 (1978).
64. A. Yariv, *IEEE J. Quantum. Electron.* **QE-14**, 650 (1978).
65. D. Bloch and M. Ducloy, *J. Phys. B* **14**, 1471 (1981).
66. M. A. Vasil'eva, J. Vischakas, V. Kabelka, and A. V. Masalov, *Opt. Commun.* **53**, 412 (1985).
67. M. Kaczmarek, J. M. Buchert, S. Kielich, and J. R. Lalanne, *J. Mod. Opt.* **38**, 193 (1991).
68. E. I. Demikhov, V. K. Dolganov, and V. M. Filev, *Pis'ma Zh. Eksp. Theor. Fiz.* **37**, 305 (1983) (*JETP Lett.* **37**, 361 (1983)).
69. P. J. Collings (private communication).
70. N. Bloembergen, *Non Linear Optics*, Benjamin, New York, 1965, p. 147.
71. J. Reintjes and R. L. Carman, *Phys. Rev. Lett.* **28**, 1697 (1972).

72. P. G. De Gennes, *Phys. Lett.* **30A**, 454 (1969).
73. P. G. De Gennes, *Mol. Cryst. Liq. Cryst.* **12**, 193 (1971).
74. W. Maier and A. Saupe, *Z. Naturforsch.* **A14**, 882 (1959); **15**, 287 (1960).
75. W. S. Struve, *Opt. Commun.* **21**, 215 (1977).
76. B. Pouligny, E. Sein, and J. R. Lalanne, *Phys. Rev. A* **21**, 1528 (1980).
77. G. K. L. Wong and Y. R. Shen, *Phys. Rev. A* **10**, 1277 (1974).
78. E. G. Hanson, Y. R. Shen, and G. K. L. Wong, *Phys. Rev. A* **14**, 1281 (1976).
79. J. Prost and J. R. Lalanne, *Phys. Rev. A* **8**, 2090 (1970).
80. J. C. Filippini and Y. Poggi, *J. Phys. Lett.* **37**, 17 (1976).
81. M. Schadt and W. Helfrich, *Mol. Cryst. Liq. Cryst.* **17**, 355 (1972).
82. M. Brunet-Germain, *C. R. Acad. Sci. Paris* **271**, 1075 (1970).
83. G. Eyring and M. D. Fayer, *J. Chem. Phys.* **81**, 4314 (1984).
84. F. W. Deeg, J. J. Stankus, S. K. Greenfield, V. J. Newell, and M. D. Fayer, *J. Chem. Phys.* **90**, 6893 (1989).
85. F. W. Deeg and M. D. Fayer, *J. Chem. Phys.* **91**, 2269 (1989).
86. F. W. Deeg, S. R. Greenfield, J. J. Stankus, V. J. Newell, and M. D. Fayer, *J. Chem. Phys.* **93**, 3503 (1990).
87. I. C. Khoo, T. H. Liu, and P. Y. Yan, *J. Opt. Soc. Am.* **B4**, 115 (1987).
88. I. C. Khoo and R. Normandin, *Opt. Lett.* **9**, 285 (1984); *IEEE J. Quantum Electron.* **QE-21**, 329 (1985).
89. I. C. Khoo, R. Michael, and P. Y. Yan, *IEEE J. Quantum Electron.* **QE-23**, 267 (1987).
90. I. C. Khoo, R. G. Lindquist, R. R. Michael, R. J. Mansfield, and P. Lopresti, *J. Appl. Phys.* **69**, 3853 (1991).
91. H. J. Eichler and R. Macdonald, *Phys. Rev. Lett.* **67**, 2666 (1991).
92. C. Druon and J. M. Waerenier, *Mol. Cryst. Liq. Cryst.* **98**, 201 (1983).
93. D. Fekete, J. A. Yeung, and A. Yariv, *Opt. Lett.* **5**, 51 (1980).
94. P. A. Madden, F. C. Saunders, and A. M. Scott, *IEEE J. Quantum Electron.* **QE-22**, 1287 (1986).
95. J. R. Lalanne, J. Buchert, C. Destrade, H. T. Nguyen, and J. P. Marcerou, *Phys. Rev. Lett.* **62**, 3046 (1989).
96. J. R. Lalanne, C. Destrade, H. T. Nguyen, and J. P. Marcerou, *Phys. Rev. A* **44**, 6632 (1991).
97. P. Martinoty, S. Candau, and F. Debeauvais, *Phys. Rev. Lett.* **27**, 1123 (1981).
98. O. Mondain-Monval, J. R. Lalanne, and J. P. Marcerou, to be published.
99. F. C. Frank, *Discuss. Faraday Soc.* **25**, 19 (1958).
100. *Handbook of Chemistry and Physics*, 64th ed., R. C. Weast (Ed.), CRC Press, Boca Raton, FL, 1984.
101. D. A. Dunmut and W. H. Miller, *J. Phys.* **40**, 471 (1978).
102. J. D. Bunning, D. A. Crellin, and T. E. Faber, *Liq. Cryst.* **1**, 37 (1986).
103. Value taken from Ref. 36, with the assumption that the C<sub>8</sub>H<sub>17</sub> chain has an isotropic first-order polarizability in the plane perpendicular to the long molecular axis.
104. K. M. Zero and R. Pecora, *Macromolecules* **15**, 87 (1982).
105. V. I. Gajduk and Y. P. Kalmykov, *J. Chem. Soc. Faraday Trans.* **2**, 929 (1981).

106. C. W. Garland, private communication.
107. R. B. Meyer, *Mol. Cryst. Liq. Cryst.* **40**, 33 (1977).
108. H. R. Brand and H. Pleiner, *Phys. Rev. Lett.* **64**, 1309 (1990).
109. E. Freyss, private communication.
110. K. Kremer, S. U. Vallerien, H. Kapitzka, R. Zentel and E. W. Fisher, *Phys. Rev. A* **42**, 3667 (1990).
111. F. Kremer, A. Schönfeld, S. U. Vallerien, A. Hofmann, and N. Schwenk, *Ferroelectrics* **121**, 13 (1991).
112. L. Benguigui, *J. Phys.* **43**, 915 (1982).
113. R. Nozaki, T. K. Bose, and J. Thoen, *Ferroelectrics* **121**, 1 (1991).
114. C. Flytzanis and Y. R. Shen, *Phys. Rev. Lett.* **33**, 14 (1974).
115. Y. Galerne and L. Liebert, *Phys. Rev. Lett.* **64**, 906 (1990); **66**, 2891 (1991).
116. K. Hirakao, A. Taguchi, Y. Ouchi, H. Takezoe, and A. Fukuda, *Jpn. J. Appl. Phys.* **29**, L103 (1990).